

# Mantle flow in subduction systems: The mantle wedge flow field and implications for wedge processes

Maureen D. Long,<sup>1</sup> and Erin A. Wirth<sup>1</sup>

Received 12 July 2012; revised 14 December 2012; accepted 18 December 2012.

[1] The mantle wedge above subducting slabs is associated with many important processes, including the transport of melt and volatiles. Our understanding of mantle wedge dynamics is incomplete, as the mantle flow field above subducting slabs remains poorly understood. Because seismic anisotropy is a consequence of deformation, measurements of shear wave splitting can constrain the geometry of mantle flow. In order to identify processes that make first-order contributions to the pattern of wedge flow, we have compiled a data set of local *S* splitting measurements from mantle wedges worldwide. There is a large amount of variability in splitting parameters, with average delay times ranging from  $\sim 0.1$  to  $0.3$  s up to  $\sim 1.0$ – $1.5$  s and large variations in fast directions. We tested for relationships between splitting parameters and a variety of parameters related to subduction processes. We also explicitly tested the predictions made by 10 different models that have been proposed to explain splitting patterns in the mantle wedge. We find that no simple model can explain all of the trends observed in the global data set. Mantle wedge flow is likely controlled by a combination of downdip motion of the slab, trench migration, ambient mantle flow, small-scale convection, proximity to slab edges, and slab morphology, with the relative contributions of these in any given subduction system controlled by the subduction kinematics and mantle rheology. There is also a likely contribution from B-type olivine and/or serpentinite fabric in many subduction zones, governed by the local thermal structure and volatile distribution.

**Citation:** Long, M. D., and E. A. Wirth (2013), Mantle flow in subduction systems: The mantle wedge flow field and implications for wedge processes, *J. Geophys. Res. Solid Earth*, 118, doi:10.1002/jgrb.50063.

## 1. Introduction

[2] The mantle wedge above subducting slabs represents an important, yet poorly understood aspect of Earth's plate tectonic regime. As slabs of oceanic lithosphere descend and are recycled back into the mantle, a variety of processes operate in the overlying mantle wedge, including the generation and transport of melt which is responsible for the arc volcanism usually observed at the surface. Despite its importance to the plate tectonic system, many aspects of the mantle wedge remain poorly understood, including its thermal structure, the storage and transport of water and other volatiles, and the mechanisms by which melt is transported to the surface [e.g., van Keken, 2003; Wiens et al., 2008]. The pattern and vigor of mantle flow in the wedge, and the dynamic processes that operate to control that flow, also remain poorly understood. Simple 2-D corner flow induced by

viscous coupling between the downgoing slab and the overlying mantle has been invoked to explain many aspects of the mantle wedge, including its thermal structure [e.g., Kincaid and Sacks, 1997; van Keken et al., 2002; Keleman et al., 2003], the generation of melt and the location of arc volcanoes [e.g., Grove et al., 2009], the transport of volatiles [e.g., Cagnioncle et al., 2007], and a range of seismological observations such as velocities and attenuation [e.g., Wiens and Smith, 2003; Abers et al., 2006]. However, other types of flow regimes, including dominantly trench-parallel flow, have also been suggested based on numerical modeling studies [e.g., Conder and Wiens, 2007] or observations, either seismological [e.g., Smith et al., 2001; Abt et al., 2009] or geochemical [e.g., Hoernle et al., 2008; Heyworth et al., 2011].

[3] The most direct observational constraints on flow patterns in the mantle wedge come from observations of seismic anisotropy, which manifests itself clearly in the splitting or birefringence of shear waves. Anisotropy in the upper mantle is a consequence of deformation, either through the lattice-preferred orientation of mantle minerals [e.g., Karato et al., 2008] or through the shape-preferred orientation of elastically distinct material such as partial melt [e.g., Zimmerman et al., 1999; Vauchez et al., 2000]. The characterization of upper mantle anisotropy can thus shed light on the pattern of upper mantle deformation [e.g., Long and Becker, 2010]. Shear wave splitting has become a popular tool for probing deformation in subduction zones, and

All Supporting Information may be found in the online version of this article.

<sup>1</sup>Department of Geology and Geophysics, Yale University, New Haven, Connecticut, USA.

Corresponding author: M. D. Long, Department of Geology and Geophysics, Yale University, PO Box 208109, New Haven, CT 06520, USA. (maureen.long@yale.edu)

©2013. American Geophysical Union. All Rights Reserved.  
2169-9313/13/10.1002/jgrb.50063

measurements of splitting for local  $S$  phases that originate from slab earthquakes can provide relatively direct constraints on anisotropy and mantle flow above subducting slabs.

[4] While there is a wealth of published studies on  $S$  wave splitting in the mantle wedge available in the literature, consensus on how to interpret these measurements and an understanding of the pattern of mantle flow in mantle wedges have remained elusive, for several reasons. First, mantle wedge shear wave splitting patterns are highly variable in subduction zones worldwide, with large variations in average delay times and spatially variable fast directions [e.g., *Long and Silver*, 2008]. Second, direct comparisons among local  $S$  splitting studies can be difficult, because of variable station coverage in subduction zones and differences in pre-processing procedures and measurement methods. Third, unlike in many regions of the upper mantle, there is ambiguity about the interpretation of mantle wedge fast splitting directions in terms of flow geometry, since B-type olivine lattice-preferred orientation (LPO) [*Jung and Karato*, 2001; *Karato et al.*, 2008] or serpentinite LPO [*Kneller et al.*, 2008; *Katayama et al.*, 2009; *Jung*, 2011] may be present in the wedge, and there may be a contribution from aligned partial melt [*Zimmerman et al.*, 1999; *Holtzman et al.*, 2003] or from aligned cracks in the uppermost part of the slab [*Faccenda et al.*, 2008; *Healy et al.*, 2009].

[5] A promising approach to unraveling the dynamic processes that control mantle wedge anisotropy is to consider the variability in shear wave splitting patterns observed in subduction zones worldwide and to compare splitting parameters to other parameters that describe subduction in order to identify first-order controls on the global pattern of wedge splitting. *Long and Silver* [2008] recently carried out such a study and proposed a framework for subduction zone anisotropy in which the mantle wedge flow field is controlled by the interaction of two-dimensional corner flow induced by the downgoing slab and three-dimensional flow induced by trench migration. Here we expand on this previous work and present a more complete investigation of the relationships between wedge splitting parameters and other parameters that describe subduction. In a companion paper [*Long and Silver*, 2009], we have presented a detailed investigation of shear wave splitting patterns due to anisotropy beneath subducting slabs and explored the implications of our trench-migration-controlled model for mantle dynamics.

[6] The work presented here has several goals. First, we use a more detailed description of the average splitting parameters due to wedge anisotropy than that used in *Long and Silver* [2008]. Rather than relying solely on average delay time measurements due to wedge anisotropy in any given subduction zone, we have normalized our delay time estimates by the range of event depths involved in each study and have quantified the location and sense of strike-perpendicular transitions in fast directions, which are often observed in local  $S$  splitting studies [e.g., *Nakajima and Hasegawa*, 2004; *Levin et al.*, 2004]. We have also evaluated along-strike variations in wedge splitting in two subduction zones where the data coverage is dense enough to do so (Central America and Ryukyu). Second, we present a more detailed examination of the correlations between mantle wedge splitting parameters and other parameters that describe subduction, including slab dip, curvature, and seismicity; the age and thermal state of the subducting lithosphere; and

parameters related to wedge processes such as volcanic production. Third, we critically evaluate the many models that have been proposed to explain the pattern of shear wave splitting in mantle wedges and examine the predictions made by different models in light of the global data set. Finally, we discuss the implications of the global wedge shear wave splitting data set on our understanding of mantle wedge geodynamics and processes.

## 2. A Global Data Set of Shear Wave Splitting Parameters in Mantle Wedges

### 2.1. Description of Regional Studies and Results

[7] Our compilation consists of shear wave splitting estimates of local  $S$  waves for 17 different subduction zones (or subduction zone segments). Estimates are based on more than two dozen individual studies, each of which is discussed below. A sketch of average mantle wedge splitting parameters in subduction zones globally is shown in map view in Figure 1, and the observations are summarized in Table 1; additionally, a data table containing all of the splitting parameters along with estimates of other subduction-related parameters (described in section 4.1) can be found in the Supporting Information.

[8] Splitting studies of local  $S$  phases in the Tonga subduction zone have mainly relied on data from land-based stations in the Lau back arc [e.g., *Bowman and Ando*, 1987; *Fischer and Wiens*, 1996; *Fischer et al.*, 1998]. *Smith et al.* [2001] used data from both land stations and ocean bottom seismometers (OBSs) to examine local  $S$  splitting in the Tonga fore arc, Lau back arc, and Fiji Plateau. Shear wave splitting measurements made on waveforms with a characteristic period of  $\sim 3$  s revealed trench-parallel fast directions in the fore-arc region and relatively large delay times of  $\sim 1.2$  s. Fast directions rotate upon moving westward into the back arc: fast directions are nearly trench parallel (approximately N-S) in the Lau basin and trench perpendicular (or parallel to the convergence direction) west of the back arc near the Fiji Plateau. The transition in fast direction orientation from trench parallel to trench perpendicular occurs where the subducting slab is at  $\sim 350$  km depth. Event depths span from  $\sim 100$ – $600$  km, but there is no apparent trend in splitting delay time with depth. Splitting measurements made in the Lau back-arc region are consistent with results from previous studies [*Fischer and Wiens*, 1996; *Fischer et al.*, 1998].

[9] Immediately to the south in the Kermadec Islands, we use shear wave splitting measurements made by *Long and Silver* [2008] at Global Seismographic Network (GSN) station RAO. Unfortunately, the data at this island station are very noisy in the frequency band useful for local  $S$  splitting, and only a small number of usable splitting measurements were obtained. Using a band-pass filter of 0.02–0.125 Hz, shear wave splitting measurements of local  $S$  waves from events at depths  $\sim 235$  km yielded delay times of  $\sim 1$  s with generally trench-parallel fast directions, similar to measurements made to the north in Tonga [*Smith et al.*, 2001].

[10] Again moving southward, several studies have examined shear wave splitting of SKS and teleseismic  $S$  phases in the Hikurangi subduction zone off the east coast of the North Island of New Zealand [e.g., *Gledhill and Gubbins*, 1996; *Brisbourne et al.*, 1999; *Matcham et al.*, 2000; *Audoine*

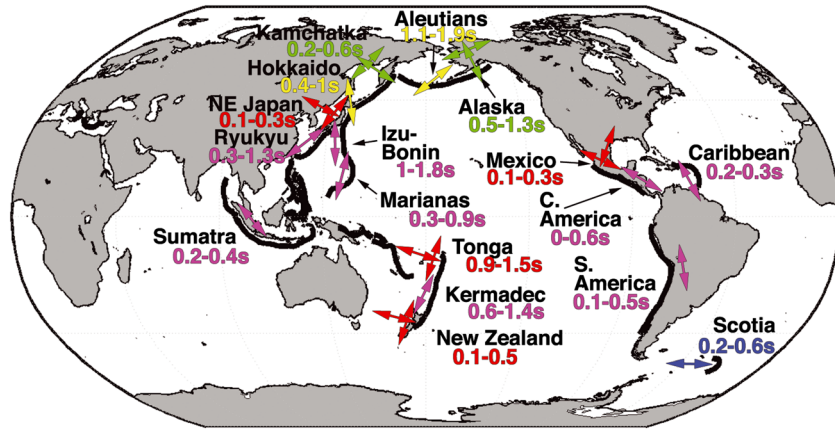


**Figure 1.** Summary map of wedge splitting worldwide. Arrows indicate the first-order patterns in average fast direction; where multiple arrows are present, this indicates a spatial transition in observed  $\phi$ . Arrows are color coded by fast direction observations; magenta arrows indicate dominantly trench-parallel  $\phi$ , blue arrows indicate dominantly trench-perpendicular  $\phi$ , yellow arrows indicate complex and variable  $\phi$ , red arrows indicate a transition from trench-parallel  $\phi$  close to the trench to trench-perpendicular  $\phi$  farther away, and green arrows indicate the opposite transition (from trench-perpendicular  $\phi$  close to the trench to trench-parallel  $\phi$  farther away). Beneath the name of each subduction zone, we indicate the range of observed delay times.

**Table 1.** Summary of Wedge Splitting<sup>a</sup>

Subduction Zone	Wedge $\delta t$ (s)	Wedge $\phi$	Event Depths (km)	Frequency Range (Hz)	Source
Tonga	$1.2 \pm 0.3$	Trench-   to trench- $\perp$	100–600	0.3 <sup>b</sup>	Smith et al. [2001]
Kermadec	$1.0 \pm 0.4$	Trench-	~235	0.02–0.125	Long and Silver [2008]
Hikurangi	$0.3 \pm 0.2$	Trench-   to trench- $\perp$	57–293	0.5–3.0	Morley et al. [2006]
Sumatra	$0.3 \pm 0.1$	Trench-	100–200	0.1–1.0	Hammond et al. [2010]
Marianas	$0.6 \pm 0.3$	Trench-	80–250	0.3–0.7	Pozgay et al. [2007]
Izu-Bonin	$1.4 \pm 0.4$	Trench-	370–502	0.02–0.125	Wirth and Long [2010]
Ryukyu	$0.8 \pm 0.5$	Trench-	80–272	0.1–1.0	Long and van der Hilst [2006]
NE Japan	$0.2 \pm 0.1$	Trench-   to trench- $\perp$	75–150	0.125–0.5	Huang et al. [2011b]
Hokkaido	$0.7 \pm 0.3$	Variable	86–474	0.125–0.5	Wirth and Long [2010]
Kamchatka	$0.4 \pm 0.2$	Trench- $\perp$ to trench-	25–150	0.5–2.0	Levin et al. [2004]
Aleutians	$1.5 \pm 0.4$	Trench-   or oblique	~100 km	0.02–0.125	Long and Silver [2008]
Alaska	$0.9 \pm 0.4$	Trench- $\perp$ to trench-	n/a <sup>c</sup>	n/a <sup>c</sup>	Christensen et al. [2003]
Caribbean	$0.27 \pm 0.03$	Trench-	128	1.0–3.0	Piñero-Felicangeli and Kendall, [2008]
Middle America	$0.3 \pm 0.3$	Trench-	30–220	0.01–2.0	Abt et al. [2009]
Mexico	$0.2 \pm 0.1$	Trench-   to trench- $\perp$	60–106	0.5–2.0	Léon Soto et al. [2009]
South America	$0.3 \pm 0.2$	Trench-	50–350	0.01–1.0	Polet et al. [2000]
Scotia	$0.4 \pm 0.2$	Trench- $\perp$	100–170	0.05–0.5	Müller [2001]

<sup>a</sup>From the published literature, as described in section 2.1. Here we have listed the most relevant citations, but additional studies are discussed in the text. For each subduction zone, we list the local  $S$  shear wave splitting delay times and fast directions, along with the range of event depths, and the frequency band used to filter the data. Fast direction descriptions that include more than one orientation describe how the orientation changes moving from the fore arc into the back arc.

<sup>b</sup>Estimated from the characteristic period of sample waveforms.

<sup>c</sup>Not reported.

et al., 2004; Marson-Pidgeon and Savage, 2004; Greve et al., 2008]. For measurements of local  $S$  splitting, we rely on results from Morley et al. [2006]. In the fore-arc region, results revealed trench-parallel shear wave splitting fast directions and an average delay time of  $\sim 0.2$  s (using a band-pass filter 0.5–3 Hz), which the authors attribute mainly to crustal anisotropy in the overriding plate. Moving into the back arc, this transitions to trench-perpendicular fast directions with delay times  $\sim 0.35$  s. This transition in measured shear wave splitting parameters occurs across the Taupo Volcanic Zone, which lies approximately 100 km above the subducting Pacific slab. Event depths ranged from

about  $\sim 50$ – $300$  km, with no apparent variation in delay time with increasing depth.

[11] For the Sumatra subduction system in an earlier version of this compilation, Long and Silver [2008] measured shear wave splitting of local  $S$  phases at permanent station PSI. We choose to focus our discussion on the more recent and extensive study by Hammond et al. [2010], but note that their results are consistent with those reported by Long and Silver [2008]. The majority of events had hypocentral depths between  $\sim 100$  and  $200$  km and produced  $S$  phases with trench-parallel fast directions. There is no documented transition in fast direction orientation; however, we note that all of

the stations are located along the island arc and are approximately the same distance away from the trench. Using a band-pass filter of 0.1–1 Hz, the measured shear wave splitting delay times span a wide range (0.1–1.3 s) but on average are relatively small ( $\sim 0.3$  s). The authors found no variation in delay time with event depth and use this observation to conclude that the mantle wedge is nearly isotropic and the observed anisotropy resides in the overriding plate.

[12] The tightest constraints on local  $S$  splitting in the Mariana subduction zone come from work done by *Pozgay et al.* [2007] using both OBSs and land-based stations. Shear wave splitting fast directions are predominantly trench parallel for events occurring at  $<250$  km depths in the fore arc, island arc, and back arc. For deeper events and splitting measurements made west of the back-arc spreading center, there is a transition to approximately absolute plate motion parallel fast directions. Because there is a large amount of scatter in the dataset, however, and because the transition in fast directions is only visible for the deep events, we did not categorize this system as one with a clear transition in fast directions and instead classified it as mainly trench parallel. Using a band-pass filter with corner frequencies at 0.3 and 0.7 Hz, the average shear wave splitting delay time for intermediate depth ( $<250$  km) events was 0.55 s in the northern segment of the arc and 0.36 s in the southern segment. Event depths ranged from  $\sim 80$  to 600 km. There is no trend in delay time with hypocentral depth, but the authors note that there is a slight indication of increasing delay time with increasing path length. Previous studies that relied mainly on land-based instruments and only a few OBS stations reported shear wave splitting fast directions that are closer to convergence parallel rather than trench parallel [e.g., *Fouch and Fischer*, 1998; *Volti et al.*, 2006]. However, these studies were done at different locations along the arc and at varying distances away from the trench, making a direct comparison difficult.

[13] Several studies have examined seismic anisotropy in the mantle wedge of the Izu-Bonin subduction system [e.g., *Fouch and Fischer*, 1996; *Anglin and Fouch*, 2005; *Wirth and Long*, 2010]. We focus mainly on measurements made by the most recent study by *Wirth and Long* [2010] in the northernmost section of the Izu-Bonin arc. Shear wave splitting measurements made using a band-pass filter of 0.02–0.125 Hz resulted in fast directions aligned to  $\sim N30^\circ W$  and delay times of  $\sim 1.4$  s. The seismic events used were deep ( $\sim 370$ – $500$  km), but no systematic variation in delay time with event depth was observed. Due to the oblique convergence of the Pacific plate, the fast direction orientation is somewhat in between trench parallel (roughly N-S) and absolute plate motion ( $\sim N60^\circ W$ ). This is consistent with results reported by *Anglin and Fouch* [2005] south of  $30^\circ N$  but inconsistent with the highly variable fast direction orientations they reported north of  $30^\circ N$ . Results from *Fouch and Fischer* [1996] are more clearly absolute plate motion parallel, but again, this is only a  $\sim 30^\circ$  variation from the fast direction measurements made by *Wirth and Long* [2010].

[14] *Long and van der Hilst* [2006] studied shear wave splitting of local  $S$  phases in the Ryukyu arc. Using a band-pass filter of 0.02–0.125 Hz, they measured significant shear wave splitting delay times of  $\sim 1.4$  s. However, they found that the measured delay times were frequency dependent, with a band-pass filter of 0.1–1 Hz yielding delay times

of  $\sim 0.8$  s. Fast direction orientations are predominantly trench parallel throughout the arc, which was attributed to the presence of B-type olivine fabric in the fore-arc mantle. Recent numerical modeling work has provided further support for this theory [*Kneller et al.*, 2008]. Events used in the shear wave splitting analysis range in depth from  $\sim 70$  to 300 km, and no systematic dependence of delay time upon event depth was observed.

[15] In Japan,  $S$  wave splitting from local events has been extensively studied [e.g., *Okada et al.*, 1995; *Fouch and Fischer*, 1996; *Nakajima and Hasegawa*, 2004; *Nakajima et al.*, 2006; *Salah et al.*, 2008, 2009; *Wirth and Long*, 2010; *Huang et al.*, 2011a, 2011b] and other phases have also been used to study wedge anisotropy [e.g., *Tono et al.*, 2009]. As is the case for the Ryukyu arc, the frequency dependence of shear wave splitting parameters has been well documented [*Wirth and Long*, 2010; *Huang et al.*, 2011b]. Therefore, we focus on those studies that made splitting measurements using frequency bands comparable to those of the other studies in this compilation ( $\sim 0.01$ – $1$  Hz). In southwest Japan, studies have revealed complex fast direction orientations that vary significantly over short lateral distances [*Fouch and Fischer*, 1996; *Salah et al.*, 2008, 2009; *Wirth and Long*, 2010]. This result is not unexpected, as SW Japan is adjacent to the triple junction of the Pacific, Philippine Sea, and Eurasian plates, resulting in complicated slab morphology and, most likely, complex mantle flow patterns. Given this complicated tectonic setting, we opt to not include SW Japan in our compilation. In NE Japan, we use recent shear wave splitting measurements made by *Huang et al.* [2011b] using a band-pass filter of 0.125–0.5 Hz (the same as the “high”-frequency band used in *Wirth and Long* [2010]). Events had hypocenter depths of 75–150 km and measured delay times of  $\sim 0.2$  s, consistent with the work of *Wirth and Long* [2010]. Fast direction orientations transition from trench parallel in the fore arc to trench perpendicular in the back arc, with the transition occurring where the slab is at  $\sim 75$  km depth. Although the authors interpret most of the fore-arc trench-parallel splitting as due to anisotropy in the crust of the overriding plate, other workers have attributed this signal to anisotropy in the mantle, with B-type olivine fabric present in the shallow wedge corner [*Nakajima and Hasegawa*, 2004]. To the north in Hokkaido, we rely on measurements made by *Wirth and Long* [2010]. Using a band-pass filter of 0.125–0.5 Hz, the average shear wave splitting delay time is  $\sim 0.7$  s, with variable fast direction orientations. Event depths ranged from  $\sim 80$  to 470 km, with no apparent relationship between event depth and delay time. Using higher-frequency energy (2–8 Hz), *Nakajima et al.* [2006] measured comparatively shorter delay times ( $\sim 0.1$ – $0.4$  s) in Hokkaido, with variable fast directions in the fore arc and fast direction orientations parallel to the downdip direction of the slab (roughly trench perpendicular) in the back arc.

[16] To the north in Kamchatka, local  $S$  splitting is most tightly constrained from work by *Levin et al.* [2004]. Using band-pass filters of either 0.1–1 Hz or 0.5–2 Hz, these authors found that majority of splitting delay times ranged from  $\sim 0.2$  to 0.6 s, with an average of 0.4 s. Fast direction orientations are trench perpendicular in the fore arc, with a transition at the  $\sim 100$  km slab contour to trench parallel in the back arc. Notably, this transition is opposite the trend that is observed in NE Japan [*Nakajima and Hasegawa*, 2004; *Huang et al.*, 2011b]. Event depths range from  $\sim 25$

to 150 km, and no depth dependence of shear wave splitting delay time is apparent.

[17] For local  $S$  splitting constraints in the Aleutian and Alaska subduction systems, we rely on work by Long and Silver [2008] and Christensen *et al.* [2003], respectively. In the Aleutian arc, shear wave splitting delay times from three permanent stations (ATKA, NIKO, and SMY) yielded average delay times of  $\sim 1.5$  s using a band-pass filter of 0.02–0.125 Hz with variable fast directions that ranged from roughly trench parallel to oblique. In Alaska, shear wave splitting of local  $S$  phases have been measured at stations of the BEAAR (Broadband Experiment Across the Alaska Range) experiment. Splitting delay times are  $\sim 0.9$  s, with fast direction orientations that transition from convergence parallel (or trench perpendicular) close to the trench, to trench parallel progressing into the back arc, around the 70–75 km slab contour [Christensen *et al.*, 2003].

[18] Shear wave splitting measurements for the Caribbean subduction zone come from work by Piñero-Felicangeli and Kendall [2008]. We restrict our discussion to measurements made at stations in the Caribbean arc (excluding stations in eastern Venezuela), on the island of Montserrat. This condition leaves us with only two usable shear wave splitting measurements, which are from the same event (128 km depth) at two different stations, and therefore, the results are not well constrained. Using relatively high-frequency energy compared to other studies in this compilation (1–3 Hz), the authors found trench-parallel fast directions and an average delay time of  $\sim 0.3$  s.

[19] Constraints on local  $S$  splitting in the Central America subduction zone come from studies using data from the TUCAN (Tomography Under Costa Rica and Nicaragua) experiment [Abt and Fischer, 2008; Abt *et al.*, 2009]. Delay times are relatively small, averaging  $\sim 0.3$  s with a band-pass filter of 0.01–2 Hz. Although variable over short lateral distances, fast direction orientations are predominantly trench parallel. However, small geographical subsets of the data show a greater coherence, and in certain areas, a transition from trench-perpendicular fast directions in the fore arc to trench-parallel fast directions in the back arc can be seen. The authors attribute the dominantly trench-parallel  $\phi$  to arc-parallel flow in the mantle wedge, which is supported by along-strike variations in isotopic ratios in arc lavas [Hoernle *et al.*, 2008]. Event depths in the Abt *et al.* [2009] study ranged from 30 to 220 km, and a clear trend of increasing delay time with increasing path length was observed.

[20] Splitting constraints for the subduction zone beneath Mexico rely on measurements made by León Soto *et al.* [2009], near the triple junction of the subducting Cocos and Rivera plates beneath the overriding North American plate. Shear wave splitting measurements from this study primarily sample the mantle wedge above the Rivera slab. Using a band-pass filter with corner frequencies at 0.5 and 2 Hz, shear wave splitting delay times of  $\sim 0.2$  s were measured. Fast direction orientations are complex, but we see some evidence of a transition from trench-parallel to trench-perpendicular orientations moving into the back arc, with the transition occurring at the projection of the 80 km slab contour at the surface. Event depths range from  $\sim 60$  to 100 km, and there is no observable depth dependence of shear wave splitting delay time.

[21] In South America, several studies have used shear wave splitting of local events to probe seismic anisotropy

in the mantle wedge [Kaneshima and Silver, 1995; Bock *et al.*, 1998; Polet *et al.*, 2000; Anderson and Zandt, 2004; MacDougall *et al.*, 2012]. In southern Peru, Kaneshima and Silver [1995] measured shear wave splitting of several different  $S$  phases, including local  $S$ . Due to the shallow dip of the slab in this region, local  $S$  phases from deep events have the potential to sample a significant portion of the sub-slab mantle. Therefore, we restrict our discussion to shear wave splitting from intermediate depth earthquakes originating in the subducting Nazca plate. Kaneshima and Silver [1995] reported average shear wave splitting delay times  $\sim 0.4$  s. Some scatter in fast direction orientation was reported in this study, but most measurements are sub-parallel to the trench. Moving south, in northern Chile and Bolivia, Polet *et al.* [2000] measured delay times of  $\sim 0.3$  s with predominantly trench-parallel fast directions (using a band-pass filter of 0.01–1 Hz). Delay times tended to increase with increasing event depth. Also in northern Chile, Bock *et al.* [1998] measured slightly shorter delay times of  $\sim 0.1$  s, but observed no consistent trend in fast direction orientation. Local  $S$  results from the CHARGE and RAMP deployments throughout Chile and Argentina yielded average delay times of  $\sim 0.26$ – $0.4$  s and fast directions that ranged from trench normal to trench parallel over short lateral distances [Anderson and Zandt, 2004; MacDougall *et al.*, 2012]. We have chosen to rely mainly on the study of Polet *et al.* [2000] as representative of South America in our compilation.

[22] The South Sandwich subduction zone lies south of South America and has remained largely unstudied. For this compilation, we rely solely on measurements from Müller [2001]. Due to the intense curvature of the subduction system, we use only those measurements from station CAND on Candlemas Island, located in the central portion of the island arc. Using a band-pass filter of 0.05–0.5 Hz and event depths ranging from  $\sim 100$  to 170 km, Müller [2001] found average splitting delay times of  $\sim 0.4$  s, with trench-perpendicular fast directions. However, we note that due to the extreme curvature of the Scotia trench, this orientation could be interpreted as close to parallel to the northern or southern segments of the trench.

[23] All of these regional studies have been synthesized into the first-order estimates of the range of delay times and the general fast direction patterns for each subduction system, shown in Table 1. We have estimated a range of delay times for each region based on individual studies; these estimates encompass most of the measured delay times and roughly represent a 95% confidence region, following Long and Silver [2008]. In addition to identifying average shear wave splitting parameters for each subduction zone, we have also evaluated along-strike variations in Ryukyu and Central America, as discussed in section 4.3.

## 2.2. Dependence of Shear Wave Splitting on Frequency and Path

[24] One of the most significant challenges in comparing shear wave splitting measurements from different studies is the variation in frequency content and path geometries of the waves analyzed. Studies have shown that shear wave splitting measurements are frequency dependent in the New Zealand [Marson-Pidgeon and Savage, 1999], Marianas [Fouch and Fischer, 1998], Ryukyu [Long and van der Hilst, 2006], and Japan [Wirth and Long, 2010] subduction systems.

Occasionally, it is possible to discern frequency dependence for measurements of finite-frequency  $S$  arrivals for the same raypath (that is, the same event-station pair) [e.g., *Wirth and Long, 2010*]. From a finite-frequency point of view, the size of the first Fresnel zone, the region over which sensitivity to anisotropic structure is greatest, increases with decreasing frequency [e.g., *Alsina and Snieder, 1995; Favier and Chevrot, 2003*]. Since the size of the first Fresnel zone is frequency dependent, in the presence of vertically or horizontally varying anisotropy, shear wave splitting measurements will be frequency dependent as well. In a subduction zone setting, where we may expect a complex mantle flow field and therefore heterogeneous anisotropy, it is unsurprising that shear wave splitting parameters may show some frequency dependence. Therefore, the variation in band-pass filters used by the individual studies in this compilation makes a comparison of shear wave splitting measurements between different subduction zones somewhat indirect.

[25] In order to investigate the nature of frequency-dependent splitting in the global dataset, we constructed a plot that shows the range of frequencies used in each study along with the range in observed delay times (Figure 2a). This figure shows that frequency dependence can indeed be discerned for mantle wedge splitting measurements; studies that include more low-frequency energy tend to have larger delay times, while studies that investigate higher frequencies tend to have smaller delay times. Interestingly, however, this effect is not seen when the delay times are corrected for the range of event depths (an approximate measure of the range of path lengths) in each study (Figure 2b). In this case, there is no obvious relationship between the amount of splitting per 100 km of path length and the frequency content of the waves under study. This suggests that at least part of the frequency effect in the global dataset is actually due to path effects rather than to finite-frequency complications due to complex structure;  $S$  arrivals that have longer paths in the upper mantle likely have more attenuation at high frequencies, and high-frequency measurements are likely sparser for deep events. Of course, individual studies have documented frequency-dependent splitting that is independent of path effects [e.g., *Wirth and Long, 2010*], so finite-frequency effects due to complex anisotropy are certainly present in some individual subduction zones. However, this does not appear to be a first-order effect globally, which suggests that our approach to constructing a global compilation that combines studies with different frequency contents should be valid, as long as the effects of path length are correctly accounted for.

[26] Another concern in combining many individual studies into a single global compilation is the effect of different raypath sampling in different subduction zones. The raypath sampling in any given wedge splitting study is controlled by the slab morphology and the distribution of stations at the surface, which differ markedly among different studies. One problem is that some studies only sample a small part of the mantle wedge, which hampers our ability to characterize (or rule out) transitions in splitting parameters in the fore-arc, arc, and back-arc regions. It is important to keep this limitation in mind, particularly when comparing fast direction patterns to tectonic parameters, as discussed below. A second challenge is that the large range in path lengths for  $S$  arrivals in different studies makes a direct comparison

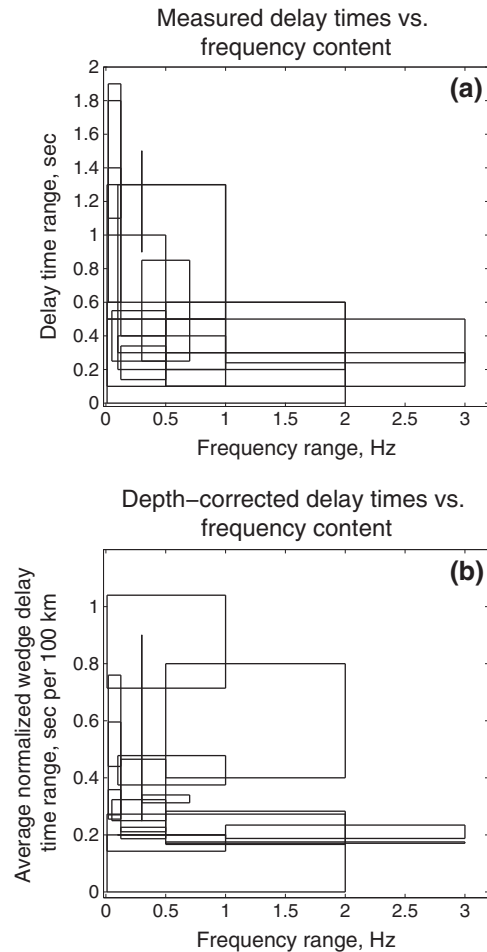


**Figure 2.** Plots of average delay time versus frequency range for the global wedge splitting data set. (a) Plot of the range of delay times versus the range of frequencies used in the analysis for each subduction system. Each region is represented with a box whose width covers the range of frequencies and whose height covers the range of delay times. (b) Plot of the range of depth-corrected delay times versus the range of frequencies. The delay time range is normalized by the range of depths in each study.

difficult. As discussed above, some studies of wedge splitting find no evidence for a dependence of  $\delta t$  on path length or event depth [e.g., *Léon Soto et al., 2009; Levin et al., 2004*] while others identify a clear relationship [e.g., *Abt et al., 2009*]. As illustrated in Figure 3, which plots the range in observed delay times against the range in event depths for each region, the global data set does show a general trend of increasing  $\delta t$  with increasing path length. Therefore, for most of the comparisons between wedge delay times and tectonic parameters presented in section 4 below, we correct the delay times using the range of event depths to obtain an estimate of seconds of splitting per 100 km of approximate path length for each region.

### 2.3. Other Constraints on Wedge Anisotropy

[27] Another common seismological technique used to place constraints on mantle wedge anisotropy is teleseismic receiver function (RF) analysis. Converted P-to-SH phases can be used to detect sharp changes in anisotropic structure

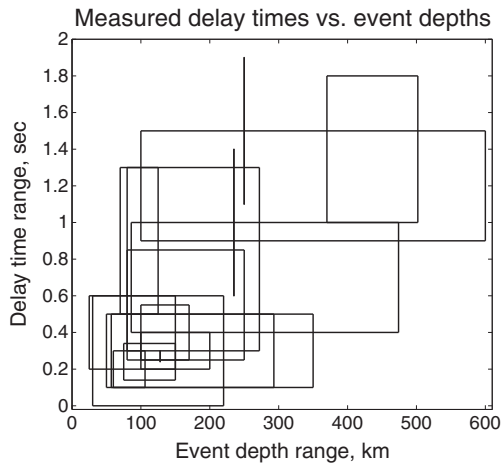


**Figure 3.** Plot of average delay times versus event depth range for the global wedge splitting data set. As in Figure 2, each subduction system is represented with a box; here the width covers the range of event depths and the height covers the range of delay times.

(or the presence of a dipping interface) in the crust or uppermost mantle directly beneath a seismic station. Backazimuthal or directional dependence (anisotropy) of such converted phases can give information regarding the orientation of anisotropy at a particular depth beneath the station [e.g., *Levin and Park, 1998*]. RF analysis can place certain constraints on anisotropic structure that are not easily inferred from methods such as shear wave splitting. For instance, one can determine the depth to anisotropic layers, non-horizontal axes of symmetry, and, through forward modeling, seismic velocities within each layer. RFs have been used to place constraints on mantle wedge anisotropy in subduction zones such as Cascadia [*Park et al., 2004; Nikulin et al., 2009*] and Japan [*Wirth and Long, 2012*]. Several of these studies have detected the contrast in anisotropic structure between the crust of the downgoing plate and the mantle wedge above it, providing constraints on the geometry of anisotropy directly above the slab. However, the interpretation and modeling of transverse component receiver functions is highly non-unique, and the method only provides information about sharp contrasts in anisotropic structure, not wedge anisotropy as a whole.

[28]  $P$  wave travel time inversions in which parameters describing anisotropy are included represent another technique that can place constraints on wedge anisotropy (as well as anisotropy in other parts of subduction systems). This technique has recently been applied in several different well-instrumented subduction zones with good raypath coverage in the wedge, including Hikurangi [*Eberhart-Phillips and Reyners, 2009*], NE Japan [*Wang and Zhao, 2008*], SW Japan [*Wang and Zhao, 2012*], and Alaska [*Tian and Zhao, 2012*]. The constraints on  $P$  wave anisotropy thus obtained are complementary to splitting studies and occasionally present conflicting views on wedge anisotropy and processes. For example, recent work on  $P$  wave anisotropy in Alaska [*Tian and Zhao, 2012*] produced evidence for trench-parallel fast directions in the shallow part of the mantle wedge, with a transition to trench-perpendicular fast directions in the deeper wedge. This model is consistent with  $S$  wave splitting observations in many subduction zones but

conflicts with the view of mantle wedge splitting in Alaska obtained from the BEAAR experiment and described above.

[29] Each of these observational techniques for constraining mantle wedge anisotropy (local  $S$  wave splitting, anisotropic receiver function analysis, and  $P$  anisotropy tomography) has its advantages and disadvantages. While  $P$  tomography and anisotropic RF analysis can provide valuable constraints on wedge anisotropy that are complementary to those obtained with shear wave splitting studies, in this paper we have chosen to focus on splitting observations. This is mostly driven by the geographical sparsity of constraints obtained with other methods; while most subductions worldwide have been interrogated using  $S$  wave splitting techniques, the other methods have been applied to fewer regions, and it is difficult to obtain a truly global picture using other types of data. We will, however, touch on results from other methods when we evaluate different models for wedge anisotropy in section 5 below.

### 3. Models for Wedge Anisotropy

[30] A large number of models for mantle wedge flow have been proposed to explain the patterns of shear wave splitting (and other seismological indicators such as velocity and attenuation structure) observed in mantle wedges worldwide. Here we describe the many models that have been proposed and briefly discuss the predictions that these models make about the expected global patterns of shear wave splitting. These descriptions will serve as a guide for the interpretation of any possible correlations between shear wave splitting and other parameters that describe subduction, as discussed in sections 4 and 5. Sketches of four of the most commonly invoked models for mantle wedge anisotropy are shown in Figure 4.

[31] In our discussions of the possible correlations between splitting parameters and other subduction parameters, we will often use plate velocities (such as convergence velocity or trench migration velocity) as proxies for the amount of finite strain produced in the mantle due to plate-driven mantle flow. While plate velocities can serve as a rough proxy for finite strain and anisotropy strength [e.g., *Long and Silver, 2008, 2009*], it is important to stress that this proxy is imperfect. The strength and geometry of the LPO of mantle minerals such as olivine is in fact controlled by finite strain [e.g., *Zhang and Karato, 1995*], and when evaluating the strength of anisotropy, it is the amount of strain rather than the plate velocity itself that is important [e.g., *Faccenda and Capitanio, 2012*]. The amount of mantle strain that results from plate-driven processes is (indirectly) related to the plate velocity, however, in that faster-moving plates are more likely to have induced larger finite strains in the mantle. Because plate velocities can be directly observed, in contrast to mantle finite strain, we use plate velocities as a (necessarily imperfect) proxy for finite strain and anisotropy strength in this paper.

[32] The simplest model for flow in the mantle wedge invokes two-dimensional corner flow (Figure 4a), with viscous coupling between the slab and the overlying mantle resulting in slab-parallel flow just above the slab and horizontal convergence-parallel flow just beneath the overriding plate. Such corner flow has a simple analytical solution [e.g., *McKenzie, 1979; Turcotte and Schubert, 1982*] and has been used to model the thermal structure of the wedge

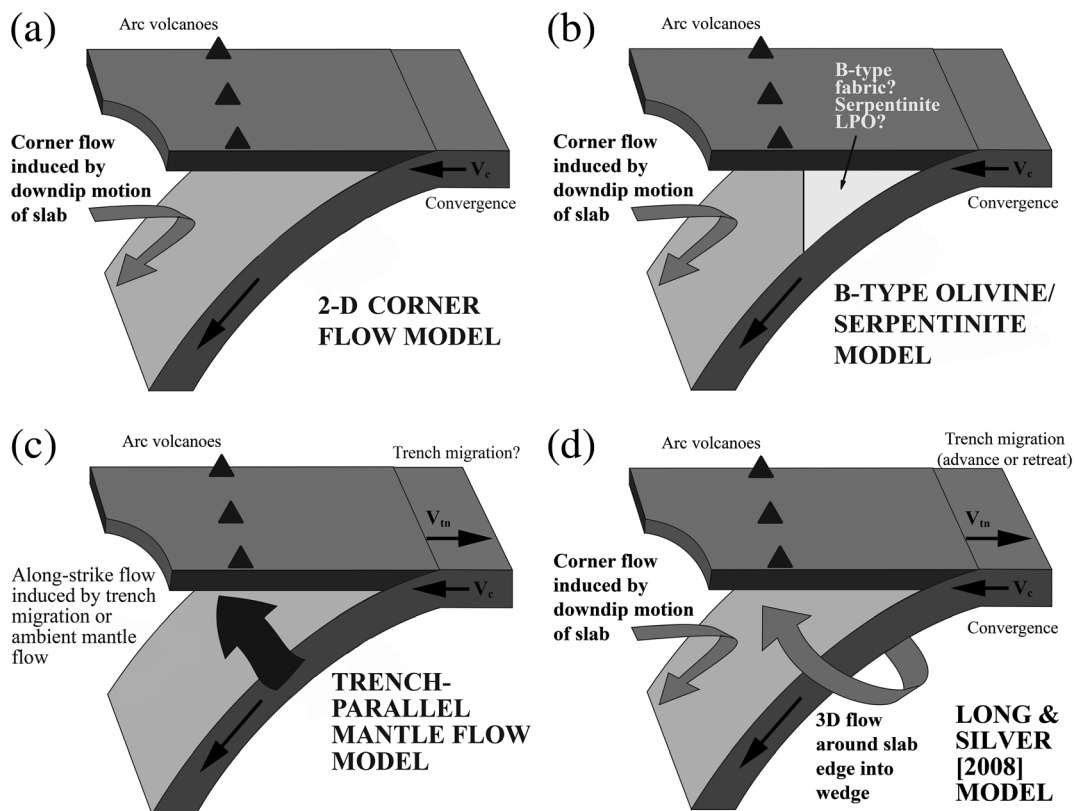


**Figure 4.** Cartoon sketches of four commonly invoked models to explain wedge anisotropy: the two-dimensional corner flow model (a), the B-type olivine and/or serpentinite LPO model (b), the along-strike flow model (c), and the model of *Long and Silver* [2008].

[e.g., *Kelemen et al.*, 2003] and the location of arc volcanoes [e.g., *Grove et al.*, 2009]. Simple numerical models of wedge corner flow that track the evolution of finite strain in the mantle wedge and make simplified predictions of the resulting anisotropy have been carried out [e.g., *Hall et al.*, 2000; *Long et al.*, 2007]. For simple olivine LPO development scenarios (e.g., A-type or similar fabric), and for the case where the local anisotropic geometry is assumed to align with the local finite strain axis, the simple corner flow model would predict dominantly trench-perpendicular fast directions. It is important to keep in mind, however, that the kinematics of corner flow involve rapid lateral transitions in flow velocities, and in this case, olivine LPO may “lag” the evolution of the finite strain ellipse [e.g., *Kaminski and Ribe*, 2002]. Models of anisotropy and the resulting shear wave splitting for “wedge-shaped” anisotropic geometries such as those that might result from simple 2-D corner flow have shown that splitting patterns may exhibit complications even for simple flow and LPO development scenarios [*Levin et al.*, 2007]. Nevertheless, if simple corner flow combined with A-type or similar olivine fabric is the dominant scenario in most mantle wedge regions, we would expect to see (1) predominantly trench-perpendicular fast directions and (2) an increase in anisotropic strength with increasing convergence velocity, if  $V_c$  values are a rough proxy for the organization and strength of the 2-D flow field [e.g., *Long and Silver*, 2008].

[33] The common observation of trench-parallel  $\phi$  in the mantle wedge, which contradicts the simplest models, has

led to alternative models for wedge anisotropy. One such model invokes the presence of B-type olivine fabric (Figure 4b), which changes by 90° the relationship between strain and the resulting fast splitting direction. Experimental work by *Jung and Karato* [2001] and *Jung et al.* [2006] has shown that B-type fabric might dominate under the conditions present in the shallow part of the mantle wedge, namely, low temperatures, high stresses, and the presence of a significant amount of water. Geodynamical modeling work has demonstrated that these conditions may predominate in much of the fore-arc mantle wedge [*Kneller et al.*, 2005, 2007] and the transition from B-type olivine in the fore-arc to A-, C-, or E-type in the rest of the wedge may be consistent with shear wave splitting patterns in several subduction zones [e.g., *Nakajima and Hasegawa*, 2004; *Long and van der Hilst*, 2006; *Lassak et al.*, 2006; *Kneller et al.*, 2008]. Some workers have suggested that B-type olivine fabrics, if they are present in the wedge, may be largely confined to a relatively thin layer directly above the slab [e.g., *Tasaka et al.*, 2008; *Katayama*, 2009]. The major first-order prediction made by the B-type fabric model is that there should be a transition from trench-parallel  $\phi$  in the fore-arc region to trench-perpendicular  $\phi$  in the back-arc region.

[34] Possible contributions to splitting from anisotropic minerals other than olivine have also been explored. Specifically, there may be a contribution to splitting from serpentinite minerals [e.g., *Kneller et al.*, 2008], which might be present in the mantle wedge as volatiles are released and hydrate the mantle above the slab [*Hilaret and Reynard*, 2008].

Serpentinite minerals such as antigorite may have very strong intrinsic single-crystal anisotropies, up to ~40% or perhaps greater [e.g., Kern, 1993; Mainprice and Ildefonse, 2009; Mookherjee and Capitani, 2011], and recent work on serpentinite LPO from experiments [e.g., Katayama *et al.*, 2009] and natural rocks [e.g., Dewandel *et al.*, 2003; van de Moortèle *et al.*, 2010; Bezacier *et al.*, 2010; Jung, 2011; Nishii *et al.*, 2011] has begun to yield a framework for relating deformation geometry and shear wave splitting observations for serpentinite minerals. As argued by Katayama *et al.* [2009], serpentinite LPO in a deformed layer above the subducting slab may produce trench-parallel fast directions and relatively large delay times (~1 s) even for a relatively thin layer (~10–20 km). If antigorite LPO represents the dominant mechanism for anisotropy in most mantle wedges, one might expect (1) widespread observations of a trench-parallel to trench-perpendicular transition in measured fast directions (as for the B-type model) with the location of the transition corresponding to the location of the breakdown in antigorite stability and (2) a relationship between delay times and subduction parameters that influence the degree of slab hydration, such as the age (and thus temperature) of the subducting slab and perhaps the slab dip, which may influence the bending stresses at the outer rise, where serpentinization of the oceanic lithosphere is likely to take place [e.g., Ranero *et al.*, 2003]. It is important to keep in mind, however, that many different parameters likely influence the degree of slab hydration and that the processes through which oceanic lithosphere is hydrated are not completely understood.

[35] Another class of model which has been proposed to explain observations of trench-parallel fast directions invokes dominantly trench-parallel mantle flow in combination with A-, C-, or E-type olivine fabric (Figure 4c). This type of model would predict trench-parallel  $\phi$  at stations located above the region of the wedge dominated by trench-parallel flow and has been invoked to explain both shear wave splitting patterns [e.g., Smith *et al.*, 2001; Pozgay *et al.*, 2007; Abt *et al.*, 2009] and geochemical trends [e.g., Turner and Hawkesworth, 1998; Hoernle *et al.*, 2008; Heyworth *et al.*, 2011] in individual subduction systems. Trench-parallel mantle flow in the wedge has been investigated from a modeling point of view by, e.g., Conder and Wiens [2007], who argued that along-strike pressure gradients, perhaps due to trench migration or ambient mantle flow, can drive trench-parallel flow in a low-viscosity region of the wedge if such a region is present. Rapid mantle flow around a slab edge may also drive a component of trench-parallel flow in some regions [e.g., Jadamec and Billen, 2010; Faccenda and Capitani, 2012]. If trench-parallel flow driven by trench migration were the primary explanation for mantle wedge anisotropy, one might expect to see a relationship between  $\delta t$  (as a proxy for the strength/coherence of trench-parallel flow and the resulting anisotropy) and trench migration rate ( $V_t$  or  $|V_t|$ ). One could also investigate whether  $\delta t$  correlates with the along-strike component of ambient mantle flow to test the hypothesis that trench-parallel flow is driven by the global background mantle flow field; in this scenario, downgoing slabs are decoupled from the wedge above them and do not themselves represent the major driver of wedge flow.

[36] Slight variations on what might be termed the “trench-parallel wedge flow” model have also been proposed; for example, it has been suggested that oblique subduction and transpression in the shallow part of the mantle wedge might

result in trench-parallel fast directions [e.g., Mehl *et al.*, 2003]. If the transpression model correctly represents the first-order control on mantle wedge anisotropy globally, one would expect to see a correlation between anisotropy strength and the amount of trench-parallel slab motion, expressed as either the subduction obliquity angle or the trench-parallel component of the convergence velocity  $V_c$ . For systems with little or no convergence obliquity, this model would predict either weak anisotropy (if the effect of 2-D corner flow is small) or anisotropy that is consistent with a simple corner flow field. Another related model for trench-parallel flow in the mantle wedge invokes three-dimensional flow caused by complex slab morphology; geodynamical modeling studies by Kneller and van Keken [2007, 2008] presented evidence that complex slab shapes can induce local trench-parallel stretching—and thus anisotropy—in the mantle wedge. Kneller and van Keken [2007] presented models for the Marianas and South American subduction systems that took into account the details of the slab shape and argued that complex slab morphology can cause local trench-parallel flow even if the motion of the downgoing plate is (sub-)perpendicular to the trench. A key prediction of these models is the dominance of trench-parallel  $\phi$  in parts of the mantle wedge that correspond geographically to regions of slab complexity. Finally, Long and Silver [2008] recently proposed a model (Figure 4d) which incorporates aspects of both 2-D corner flow and along-strike flow due to trench migration; in this model, flow in the wedge is controlled by a competition between 2-D flow induced by downdip motion of the slab (as parameterized by the convergence velocity,  $V_c$ ) and trench-parallel flow induced by trench migration (as parameterized by the trench migration velocity,  $V_t$ ). This model predicts that subduction systems that are either dominated by convergence (low values of  $V_{\text{norm}} = |V_t|/V_c$ ) or dominated by trench migration (high  $V_{\text{norm}}$ ) would tend to have large delay times, while systems with intermediate values of  $V_{\text{norm}}$  would tend to exhibit weak splitting.

[37] Yet another class of models that has been proposed to describe the mantle flow field in subduction zone mantle wedges invokes along-strike changes in the flow field on relatively small length scales. The concept of small-scale convection has been extensively explored in the context of cooling oceanic lithosphere, where small-scale dynamic instabilities develop beneath the lithosphere [e.g., Richter and Parsons, 1975; Buck, 1985; Korenaga and Jordan, 2003; Landuyt and Ierley, 2012]. It is less well understood under what conditions small-scale convection might occur in the mantle wedge above subducting slabs, although a few recent numerical modeling studies have been carried out [e.g., Honda and Yoshida, 2005; Honda, 2011; Wirth and Korenaga, 2012]. The work of Wirth and Korenaga [2012] suggests that mantle wedge viscosity exerts the strongest control of any subduction parameter on whether or not small-scale convection develops; unfortunately, viscosity is among the least well-constrained parameters for the wedge, although it is presumably affected by temperature (via the age, dip, and velocity of the subducting slab, among other parameters), volatile content, and degree of partial melting. The effect of small-scale convection on shear wave splitting patterns in the wedge has not yet been explored in detail, although recent work by Morishege and Honda [2011] predicted  $P$  wave anisotropy for small-scale convection models.

[38] In a similar vein, *Behn et al.* [2007] proposed a model for wedge anisotropy that invokes the foundering of gravitationally unstable lower crustal material beneath the arc as the major control on mantle wedge flow. In this model, for cases where the wedge viscosity is low and lower crustal material has a significant density anomaly, wedge flow may be dominated by small-scale downwellings and the resulting anisotropy is likely complex, with finite strain directions that are often trench-parallel beneath the arc (with a transition to convergence parallel in the back arc). Models that invoke small-scale flow processes would likely result in anisotropy that varies dramatically over short length scales in the wedge. Particularly for longer-period waves with larger Fresnel zones, such complicated anisotropy may be effectively isotropic (or only weakly anisotropic) over the length scales that are relevant for seismic waves. If small-scale convection or crustal foundering were the dominant mechanism for wedge flow in most subduction zones worldwide, we would generally expect to see low delay times that reflect this weak effective anisotropy.

[39] The models described so far invoke solid-state flow in the wedge in combination with LPO of mantle minerals (dominated by either olivine or serpentinite minerals such as antigorite) as the primary control on wedge anisotropy. However, a few alternatives to this view have been proposed, in the form of models that invoke some type of shape-preferred orientation (SPO). For example, in regions of the mantle wedge where small amounts of partial melt is present and the melt has been aligned by deformation, the medium will have an effective anisotropy on the scale relevant for seismic wavelengths due to melt SPO [e.g., *Zimmerman et al.*, 1999; *Vauchez et al.*, 2000; *Holtzman and Kendall*, 2010]. There is experimental evidence that the presence of melt, in addition to providing an SPO effect, might also affect the geometry of olivine LPO in the surrounding matrix [*Holtzman et al.*, 2003], although the geodynamical interpretation of this experimental result is debated [*Karato et al.*, 2008]. This type of model would predict a sharp transition in splitting behavior from the fore arc to the arc to the back arc; presumably, the region directly beneath the arc will be the richest in partial melt. This transition would likely take the form of high delay times directly at the arc, with weak or negligible splitting (or, if anisotropy is controlled by other processes such as corner flow elsewhere, with a distinct splitting pattern) elsewhere in the wedge. The melt SPO model would also predict that average delay times might correlate with the amount of partial melt in each wedge; the volcanic production at each arc is a reasonable (though imperfect) proxy for this variable. Another model that invokes an SPO-type mechanism to explain subduction zone anisotropy is that of *Faccenda et al.* [2008], who proposed that aligned serpentinitized cracks in the shallow part of subducting slabs might produce a combined SPO and LPO effect that explains the first-order pattern of SKS splitting in subduction systems (mainly trench-parallel fast directions, with delay times up to  $\sim 1.0$ – $1.5$  s). This model may be relevant to our understanding of shear wave splitting patterns for the mantle wedge; if some local  $S$  splitting measurements are made for earthquakes that are deep enough in the subducting slab (i.e., in the lower plane of a double Wadati-Benioff zone), then they may sample such anisotropy.

## 4. Comparison Between Splitting Parameters and Other Tectonic Parameters

### 4.1. Compilation of Subduction Parameters

[40] We have compiled a variety of parameters that describe subduction zone morphology and kinematics for comparison with local  $S$  splitting measurements. We used values of convergence velocity, descent rate, plate age, dip, thermal parameter, and depth to the slab beneath the volcanic arc from *Syracuse and Abers* [2006]. We have tested several different values for trench migration velocity based on a variety of different plate motion models and reference frames from studies by *Heuret and Lallemand* [2005], *Lallemand et al.* [2008], and *Schellart et al.* [2008]; in this paper, we focus the HS3-Nuvel1A model as compiled by *Schellart et al.* [2008], but a detailed discussion of reference frame issues is found in *Long and Silver* [2009]. For regions where the trench migration values varied rapidly along-strike, we averaged several data points in the immediate vicinity of the study area. For consistency, we used the trench migration values presented in *Long and Silver* [2008] for most subduction systems. However, in subduction zones where we used different studies to characterize the anisotropy than the *Long and Silver* [2008] compilation, we often found it more appropriate to average trench migration rates over a slightly different segment of the trench. We used values of the overriding plate stress state from *Heuret and Lallemand* [2005]. Values of the maximum depth extent of seismicity and the maximum upper mantle depth extent of the slab as imaged by seismic tomography were taken from *Lallemand et al.* [2008]. Estimates of the subduction zone radius of curvature were taken from *Tovish and Schubert* [1978] and *Jarrard* [1986]. Values of volcanic production were taken from *Reymer and Schubert* [1984]. Finally, we estimated the distance from each region of study to the slab edge from bathymetry data using GeoMapApp (<http://www.geomapapp.org/>). A file containing all of the parameter estimates for each subduction zone in our compilation can be found in the Supporting Information.

### 4.2. Exploratory Comparisons Between Splitting and Tectonic Parameters

[41] As previously done for the sub-slab case [*Long and Silver*, 2009], here we present comparisons between the average wedge splitting parameters (delay time and fast direction orientations) for each subduction segment and other parameters describing subduction. For the delay time comparison, we have normalized the range of observed delay times by the range of event depths in each study, so we actually compare the average normalized wedge delay time (expressed as seconds of splitting per 100 km of approximate path length) to 16 different tectonic parameters. These comparisons are shown in Figure 5. We have calculated the correlation coefficients ( $R$ ) for each set of variables, shown in the upper right corner of the plots in Figure 5.

[42] Unlike the sub-slab case documented in *Long and Silver* [2009], these comparisons did not yield any striking quasi-linear correlations between delay times and tectonic parameters. Indeed, for most subduction parameters we tested, there is no relationship at all with the path-corrected splitting delay times. Tested parameters that showed no obvious relationship include downgoing plate age (Figure 5d),

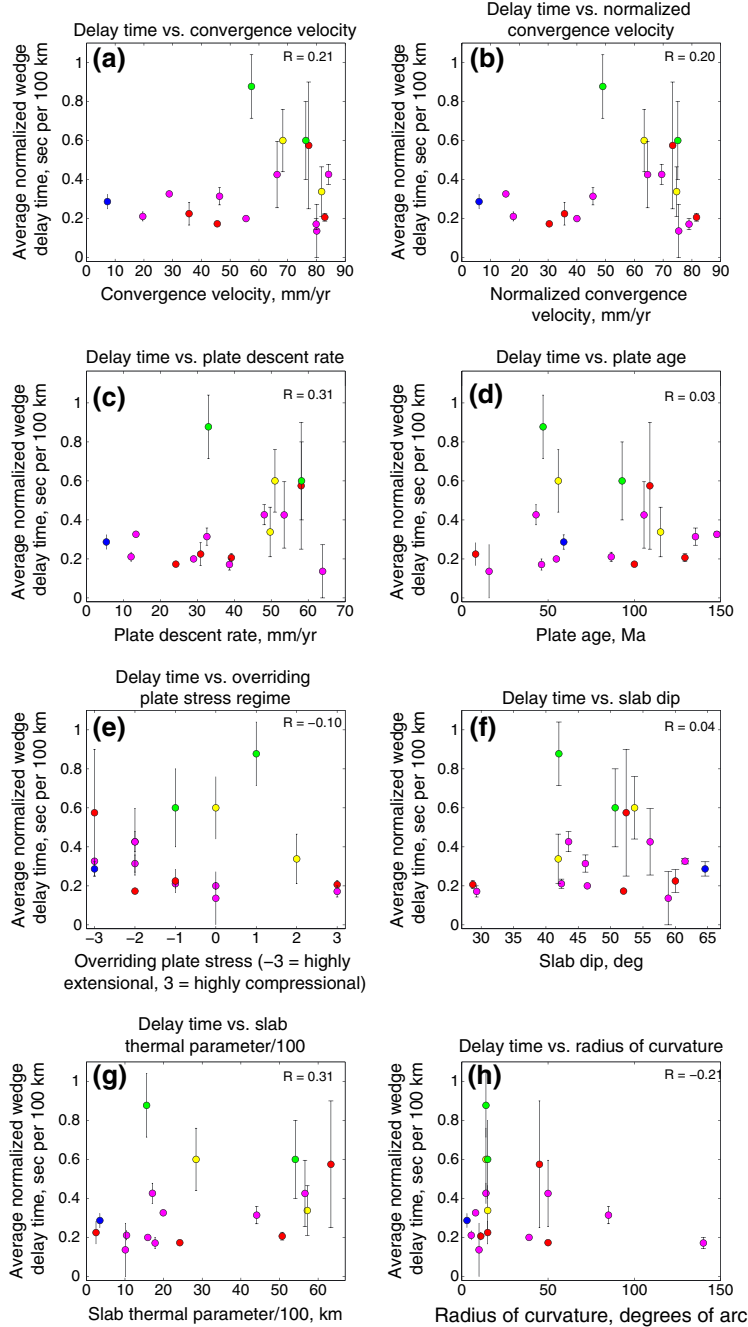


**Figure 5.** Average path-corrected wedge delay times plotted against a variety of parameters describing subduction. For each subduction system, we have normalized the range of delay times by the range of event depths used in each study, to provide a rough approximation of splitting delay time per 100 km of path length. Symbols are color coded to represent the first-order pattern of fast directions. As in Figure 1, magenta represents dominantly trench-parallel splitting, red represents a transition from trench-parallel  $\phi$  close to the trench to trench-perpendicular further away from the trench, yellow represents complex and/or oblique fast directions, green represents a transition opposite in sense to those shown in red (that is, trench-perpendicular  $\phi$  closer to the trench and trench-parallel  $\phi$  further away), and blue represents dominantly trench-perpendicular  $\phi$ . We plot delay times as a function of convergence velocity (a), trench-normal convergence velocity (b), plate descent rate (c), downgoing plate age (d), overriding plate stress regime (e), slab dip (f), slab thermal parameter (g), radius of curvature (h), distance from slab edge (i), maximum depth of seismicity (j), maximum slab penetration depth (k), depth to volcanism at arc (l), volcanic production (m), trench migration rate in the HS3-Nuvell1A reference frame (n), absolute value of trench migration rate (o), and  $V_{\text{norm}}$ , which represents the absolute value of the trench migration rate normalized by the total convergence velocity (p). Note that the  $x$  axis in Figure 5p uses a log scale. In each plot, the correlation coefficient between the two variables is shown in the upper right.

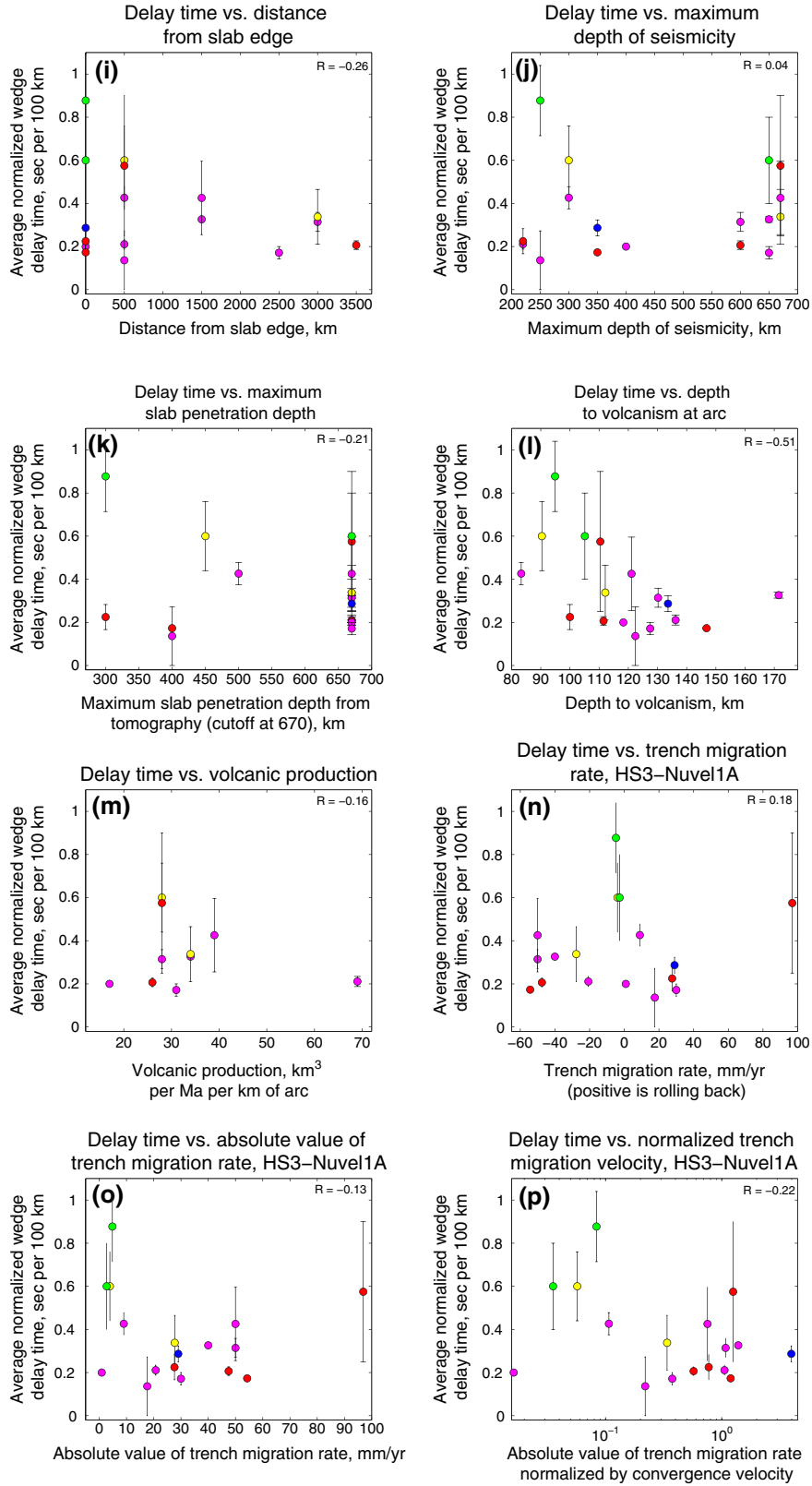


Figure 5. (continued)

overriding plate stress regime (Figure 5e), slab dip (Figure 5f), slab thermal parameter (Figure 5g), radius of curvature (Figure 5h), maximum depth of seismicity (Figure 5j), maximum slab penetration depth (Figure 5k), volcanic production

(Figure 5m), and trench migration rate in a Pacific hotspot reference frame (Figure 5n). For the other parameters we tested, there are no obvious linear or nearly linear relationships such as the one between sub-slab delay time and absolute value of

trench migration rate documented by *Long and Silver* [2008, 2009], but we can discern a few general patterns. For example, plots of path-corrected  $\delta t$  versus convergence velocity, trench-normal convergence velocity, and plate descent rate (three closely related parameters shown in Figures 5a–5c) all show a similar trend. Figure 5a demonstrates that subduction systems with lower convergence velocities  $V_c$  (less than  $\sim 55$  mm/yr) have uniformly low delay times (less than  $\sim 0.3$  s per 100 km of path), while delay times for systems with higher  $V_c$  (greater than  $\sim 60$  mm/yr) have much more variable delay times that range up to  $\sim 0.9$  s per 100 km. All of the systems with path-corrected  $\delta t$  values greater than 0.4 s per 100 km occur in systems with fast convergence. (It should be noted, however, that there are several systems with large  $V_c$  that have small delay time values.) Similar trends are evident in the plots of delay time versus trench-normal  $V_c$  and delay time versus plate descent rate, which takes into account the dip of the slab.

[43] We can also discern a hint of a trend in the plot of corrected delay time versus average distance from the nearest slab edge, shown in Figure 5i. This plot demonstrates that most of the subduction systems with particularly large  $\delta t$  values tend to be located near slab edges; specifically, each of the four regions with delay times larger than 0.5 s per 100 km is located within  $\sim 500$  km of the nearest slab edge. In contrast, all of the regions located far ( $>2500$  km) from a slab edge have relatively low delay times (less than  $\sim 0.3$  s per 100 km). However, this relationship is not simple, as we also document five systems which have small delay times despite being located near a slab edge (lower left corner of plot in Figure 5i). It is important to keep in mind that many of the studies included in our compilation extend over a large along-strike region and the average value for the distance to slab edge does not encapsulate this large range for these systems. A more detailed discussion of along-strike variations and the relationships between  $\delta t$  and slab edge proximity is found below in section 4.3.

[44] The calculated correlation coefficients for each variable shown in Figure 5 demonstrate that there are no strongly linear relationships between average delay time and subduction-related parameters. The highest  $R$  value that we obtained ( $R = -0.51$ ) was for the depth to the slab at the volcanic arc ( $H$ ), shown in Figure 5l. There is a weak trend of decreasing path-corrected  $\delta t$  values and increasing depth to slab, although there is also plenty of scatter in this trend and exceptions to it. Globally,  $H$  has been found to have a weak correlation with slab dip [*Syracuse and Abers*, 2006], so it is interesting to note that we do not observe any discernable relationship between  $\delta t$  and dip in our study (Figure 5f).

[45] Finally, we note that there are two quantities related to trench migration that display weak trends when compared with path-corrected delay time values. We have previously [*Long and Silver*, 2008] documented a relationship between  $\delta t$  (not corrected for path lengths) and the quantity  $V_{\text{norm}}$ , which represents the absolute value of the trench migration rate,  $|V_t|$ , normalized by the convergence velocity,  $V_c$ . In Figures 5n–5p, we investigate whether there are relationships between path-corrected delay time values and quantities related to the trench migration velocity. Figure 5n shows a plot of path-corrected  $\delta t$  versus trench migration rate (as calculated by *Schellart et al.* [2008] for HS3-NuvellIA); there is no clear relationship between these quantities. However, there is a somewhat clearer trend visible in Figure 5o,

which shows path-corrected  $\delta t$  versus  $|V_t|$ , where systems with either very low ( $<10$  mm/yr) or very high ( $>90$  mm/yr) trench migration rates, while systems with intermediate trench migration rates tend to have lower  $\delta t$  ( $\sim 0.2$ – $0.3$  s per 100 km). We also investigated the relationship between path-corrected  $\delta t$  and  $V_{\text{norm}}$ , which *Long and Silver* [2008] used previously to propose a global model for mantle flow in subduction systems. This previous paper documented a clear trend in which systems with either very high or very low values of  $V_{\text{norm}}$  (and were therefore either convergence dominated or trench migration dominated) tended to have large delay times, while systems with intermediate values of  $V_{\text{norm}}$  (in which convergence and trench migration velocities were roughly equal) tended to have lower delay times. The relationship shown in Figure 5p, where  $\delta t$  is now corrected for path length, is considerably less clear than the one documented in *Long and Silver* [2008].

[46] In order to further quantify the statistical relationships between anisotropy strength and other subduction-related parameters (Figure 5), we carried out additional tests of the predictive power of different subduction variables (and combinations of variables). Specifically, we carried out multiple-parameter linear regression with all possible combinations of two variables and calculated the coefficient of determination (or squared correlation coefficient),  $R^2$ . We were not able to identify any combination of two variables that led to a strikingly good fit. The three best fitting combinations were depth to the slab at the arc and slab thermal parameter ( $R^2 = 0.37$ ), depth to the slab at the arc and overriding plate stress ( $R^2 = 0.34$ ), and slab thermal parameter and distance to the slab edge ( $R^2 = 0.32$ ), but these correlations are weak and represent only a slight improvement over the best single-parameter linear regression result (depth to slab at the arc; Figure 5). Because some of the models discussed here would predict relationships between subduction variables and anisotropy strength that are more complicated than a linear relationship [e.g., the model of *Long and Silver*, 2008], we also carried out polynomial fitting for second- and third-order polynomials and tested which variables yielded the best fit (represented by a  $\chi^2$  goodness of fit measure). For second-order polynomials, the depth to the slab at the arc yielded the lowest  $\chi^2$  value, followed closely by the absolute value of the trench migration rate and less closely by the slab dip. For third-order polynomials, the depth to the slab at the arc again performed the best, followed by the absolute value of the trench migration rate and the trench-normal convergence velocity. Taken together, these statistical tests suggest that trench migration, plate convergence, and the thermal state of the slab (which likely has a strong effect on the depth of the slab beneath the volcanic arc [*Grove et al.*, 2009]) play the most important roles in controlling the strength of wedge anisotropy.

[47] We have also tested for relationships between the fast direction patterns and the same tectonic parameters discussed above; these relationships are shown in Figure 6. To construct these plots, we have placed each subduction zone into a (highly simplified) classification system that encapsulates the first-order behavior of measured fast directions. Each system is assigned an integer value from 1 to 5, where 1 indicates dominantly trench-parallel fast directions and 5 indicates dominantly trench-perpendicular fast directions. A value of 2 indicates a spatial transition from trench-parallel  $\phi$  close to

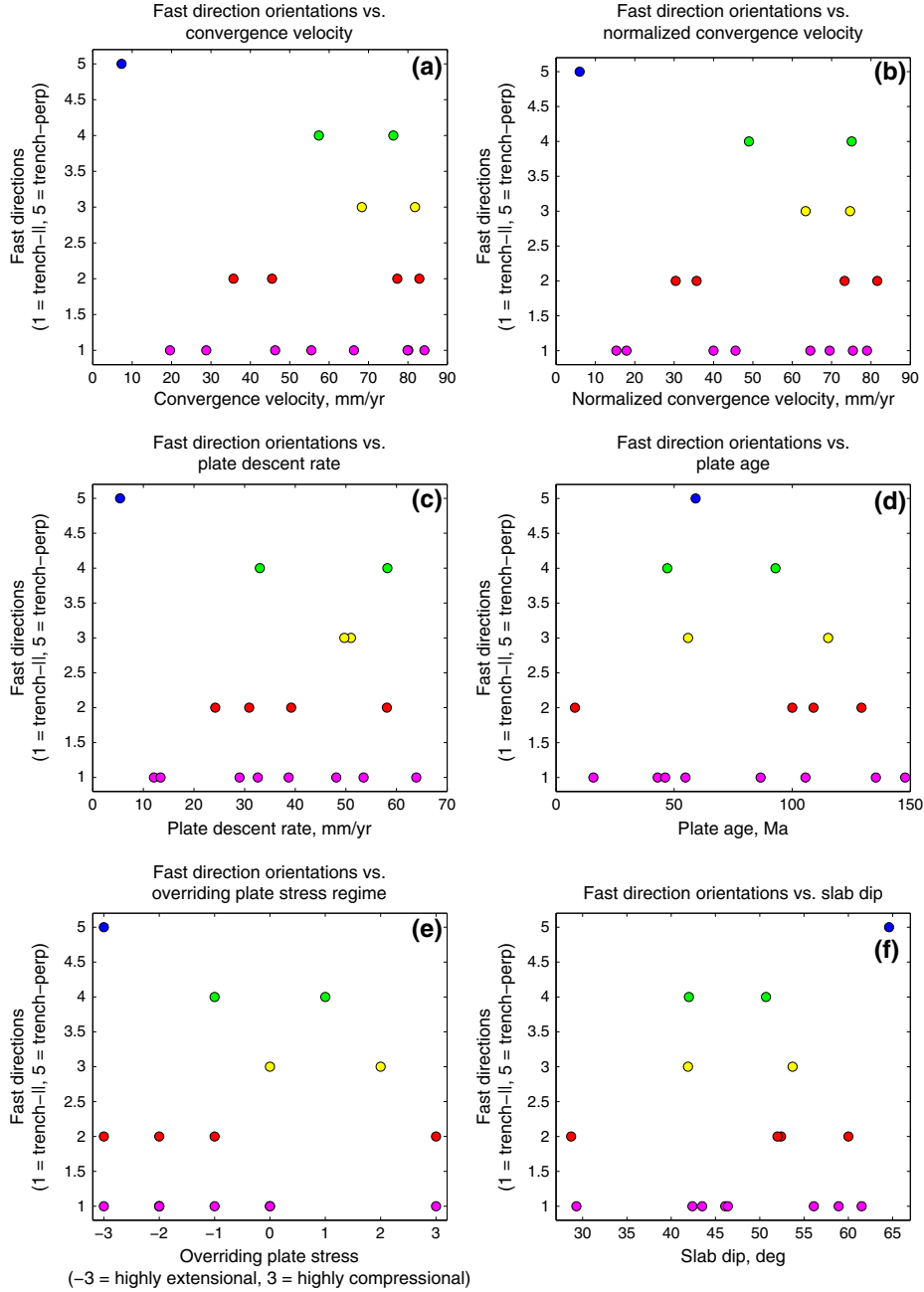


**Figure 6.** Fast direction patterns plotted against a variety of parameters describing subduction. To quantify fast direction patterns, we have assigned each system an integer value from 1 to 5, where 1 indicates dominantly trench-parallel fast directions and 5 indicates dominantly trench-perpendicular fast directions. A value of 2 indicates a spatial transition from trench-parallel  $\phi$  close to the trench to trench-perpendicular  $\phi$  further from the trench, while a value of 4 indicates the opposite transition. A value of 3 indicates fast directions either that are highly spatially variable or that are oblique to the trench strike. Symbols are also color coded according to the fast direction pattern, using the same convention as Figures 1 and 5. As in Figure 5, we plot fast directions as a function of convergence velocity (a), trench-normal convergence velocity (b), plate descent rate (c), downgoing plate age (d), overriding plate stress regime (e), slab dip (f), slab thermal parameter (g), radius of curvature (h), distance from slab edge (i), maximum depth of seismicity (j), maximum slab penetration depth (k), depth to volcanism at arc (l), volcanic production (m), trench migration rate in the HS3-Nuvell1A reference frame (n), absolute value of trench migration rate (o), and  $V_{\text{norm}}$ , which represents the absolute value of the trench migration rate normalized by the total convergence velocity (p). Note that the  $x$  axis in Figure 6p uses a log scale.

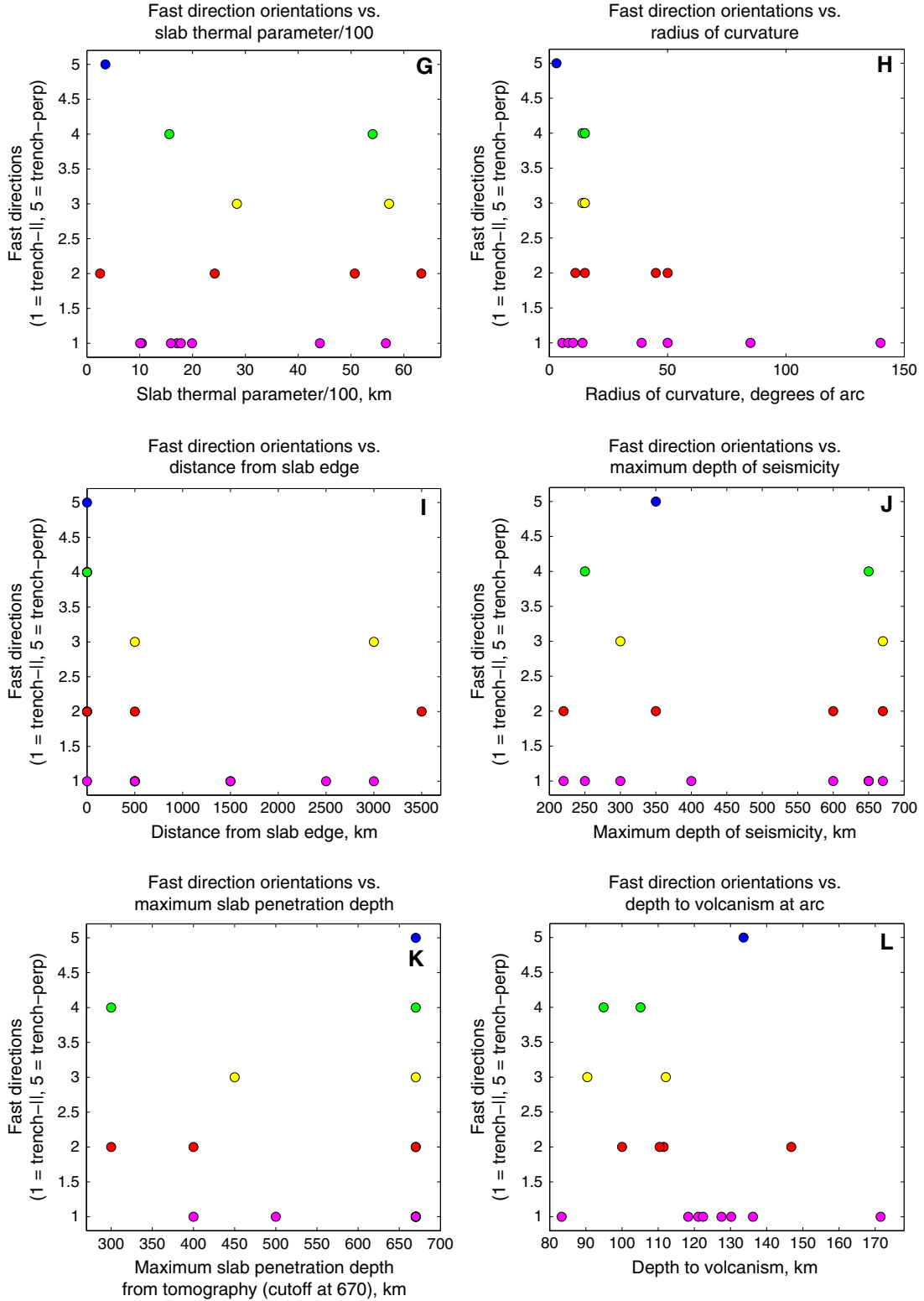
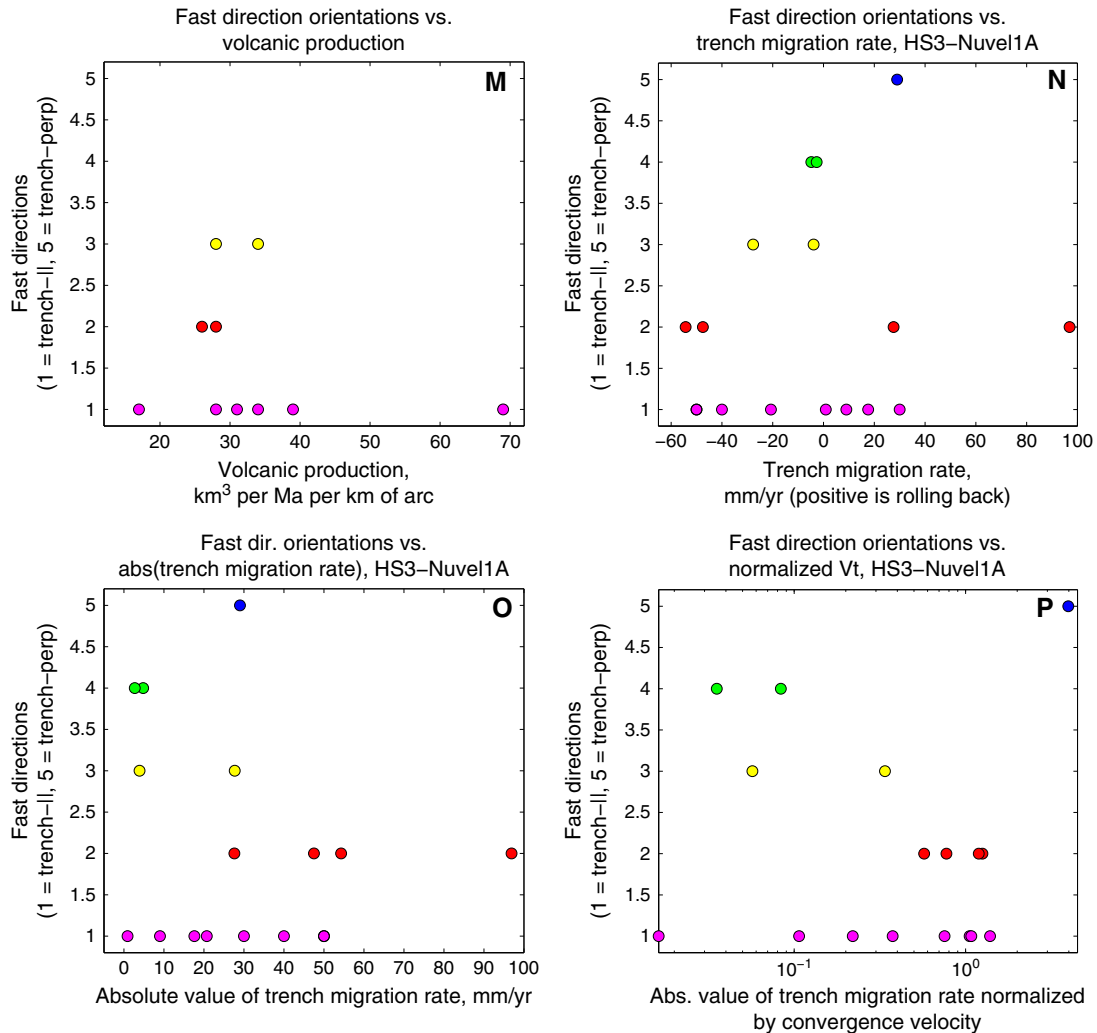


Figure 6. (continued)

the trench to trench-perpendicular  $\phi$  further from the trench, while a value of 4 indicates the opposite transition. A value of 3 indicates fast directions that are either highly spatially variable or oblique to the trench strike and thus not easily classifiable as either mostly trench parallel or mostly trench perpendicular. Of the 17 subduction systems in our data set,

the majority (12, or 71%) fall into either Category 1 or Category 2, and therefore, trench-parallel fast directions tend to dominate the observations globally, as for the sub-slab anisotropy case [Long and Silver, 2009].

[48] As Figure 6 demonstrates, this type of comparison is less successful at identifying general trends than the


**Figure 6.** (continued)

comparison with delay times described above. For nearly every subduction parameter examined, we found no evidence for an obvious relationship with fast direction patterns. Perhaps the most notable feature of the plots shown in Figure 6 is that for every parameter tested, systems that fall into fast direction Category 1 (dominantly trench-parallel fast directions), the most common behavior, cover a wide range of values for that parameter.

[49] The only parameter that exhibits even a weak relationship with fast direction patterns is the trench radius of curvature, which is shown in Figure 6h. As with other parameters, we find that dominantly trench-parallel fast directions are found in a variety of trench geometries, including both highly curved and nearly straight trenches. It is notable, however, that systems in Category 3, 4, or 5, which deviate from the most commonly observed patterns, are all associated with relatively small radii of curvature (that is, highly curved trenches).

#### 4.3. Along-Strike Variations in Splitting Behavior

[50] While average wedge splitting parameters for individual subduction zones are useful, it is also desirable to investigate along-strike variations in wedge splitting in individual

subduction systems. Unfortunately, many of the available data sets do not have good along-strike coverage. Here we focus on analyzing along-strike variations in splitting patterns for the Ryukyu and Central America subduction zones, two regions with relatively good along-strike coverage from either permanent (Japan) or temporary (Central America) stations. In particular, we look for along-strike variations in shear wave splitting fast direction orientation and delay time that may correlate with variations in convergence velocity, slab dip angle, plate age, trench migration rate, and distance to the slab edge.

[51] We used the work of *Long and van der Hilst* [2006] to study along-strike variation in the Ryukyu arc. We divided the arc into three segments (northern, central, and southern) and averaged the shear wave splitting fast direction orientations and delay times in each segment (Figure 7a). The northern and central segments contain predominantly trench-parallel fast directions. In the southernmost portion of the arc near the slab edge, the trench is highly curved, and therefore, it is unclear whether the southernmost segment exhibits trench-parallel fast directions (relative to the trench orientation to the east) or trench oblique fast directions (relative to the trench orientation to

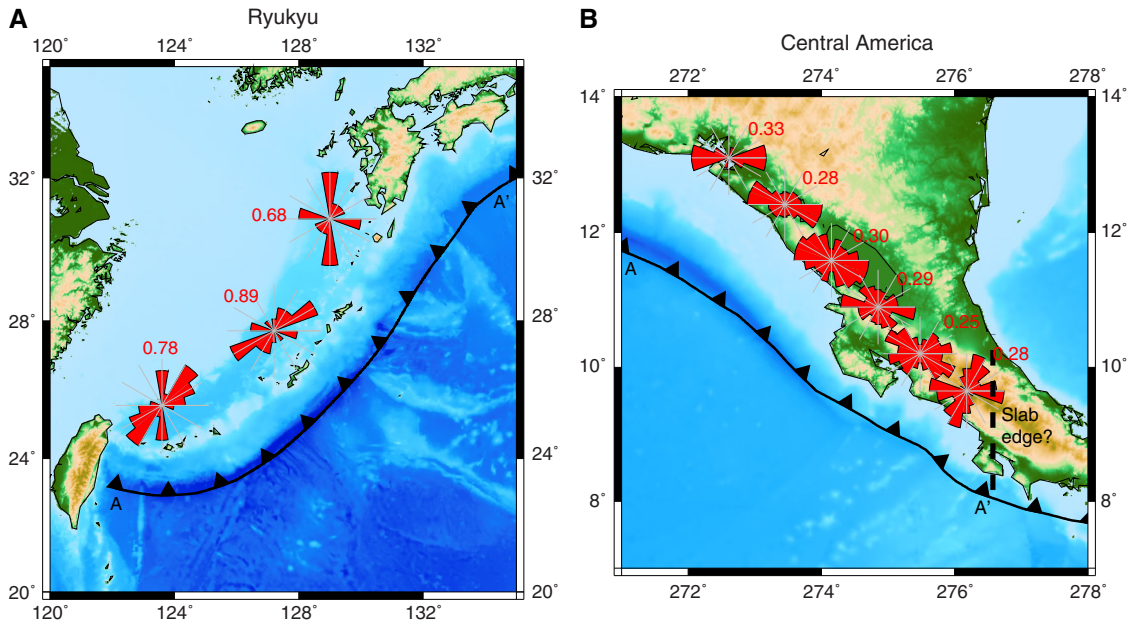


**Figure 7.** Map view of along-strike variations in delay time and fast direction for the Ryukyu (a) and Central America (b) subduction zones. For each segment, we show a rose diagram that represents a circular histogram of all fast direction measurements along with an average delay time (in seconds).

the south). There is no obvious trend in delay time along-strike (Figure 8a), with average delay times in each of the segments differing by two-tenths of a second or less.

[52] Subduction parameters in the Ryukyu arc also vary along-strike (Figure 8a). Trench-normal (that is, obliquity corrected) convergence velocity increases along-strike moving southwards (towards the slab edge) from about 65 to 80 km/Ma but then decreases to 60 km/Ma at the southernmost arc segment due to the change in trench curvature [Syracuse and Abers, 2006]. Slab dip decreases from roughly 60° to 40°, and slab age increases from about 25 Ma to 40 Ma. The trench is advancing at ~3 cm/yr in the northern half of the arc, but this decreases moving southwards and eventually switches to trench rollback (~2 cm/yr) in the southernmost segment [Schellart *et al.*, 2008]. The study area spans about ~1000 km, with the southwesternmost station located ~150 km from the slab edge. Despite the clear along-strike variations in subduction parameters in the Ryukyu subduction system, there are no obvious correlations between these variations and variations in shear wave splitting parameters (Figure 8a).

[53] Results from *Abt et al.* [2009] were used to analyze along-strike variations in the Central America subduction zone beneath Costa Rica and Nicaragua (Figure 7b). We divided the arc into six segments of length 100 km along-strike. Five of the six segments reveal roughly trench-parallel fast directions, with the sixth southeasternmost segment (closest to the slab edge) exhibiting trench-perpendicular or oblique fast directions. Most of the segments exhibit some variability in fast direction orientation. However, we note that in certain areas, the authors detect a transition from trench-perpendicular fast directions in the fore arc to trench-parallel fast direction in the back arc, and we do not differentiate between the measurements made in the fore arc and back arc in our along-strike analysis. We observe no along-strike trends in shear wave splitting delay time.

[54] The Central American subduction zone does exhibit along-strike variations in several subduction parameters (Figure 8b). Convergence velocity decreases from about 70 km/Ma to 65 km/Ma and then increases again to 80 km/Ma towards the southeast (closer to the slab edge). The slab dip increases slowly moving southeast from ~60° to 65° but then abruptly decreases back to 45°. Plate age at the trench is about 15–20 Ma and shows little along-strike variation. The trench is rolling back at ~2 cm/yr in the northern half of the arc, and this decreases slightly to ~1 cm/yr in the southern half [Schellart *et al.*, 2008]. The study region spans ~500 km, with the southeasternmost stations ~100 km from the proposed slab edge. As with Ryukyu, there are no obvious correlations between the along-strike variation in subduction parameters and along-strike variations in either delay time or fast direction distributions.

[55] Both the Ryukyu and Central America subduction zones exhibit evidence of along-strike variation, with predominantly trench-parallel fast directions everywhere except for close to the slab edge, where the fast direction orientation becomes either trench-perpendicular or oblique. Both of the subduction zones also show increasing convergence velocities moving towards the slab edge. While it may be expected that a faster convergence velocity would lead to more coherent wedge flow, toroidal flow around the slab edge due to trench migration may complicate this argument, as discussed below.

#### 4.4. Additional Tests

[56] In addition to the exploratory comparisons discussed in section 4.2 and the regional views discussed in section 4.3, we have carried out several additional tests (Figure 9) that are driven by the specific model predictions described in section 3. We investigated plots of non-path-length-corrected  $\delta t$  as a function of slab age (Figure 9a) and dip (Figure 9b), which are relevant for testing the serpentinite

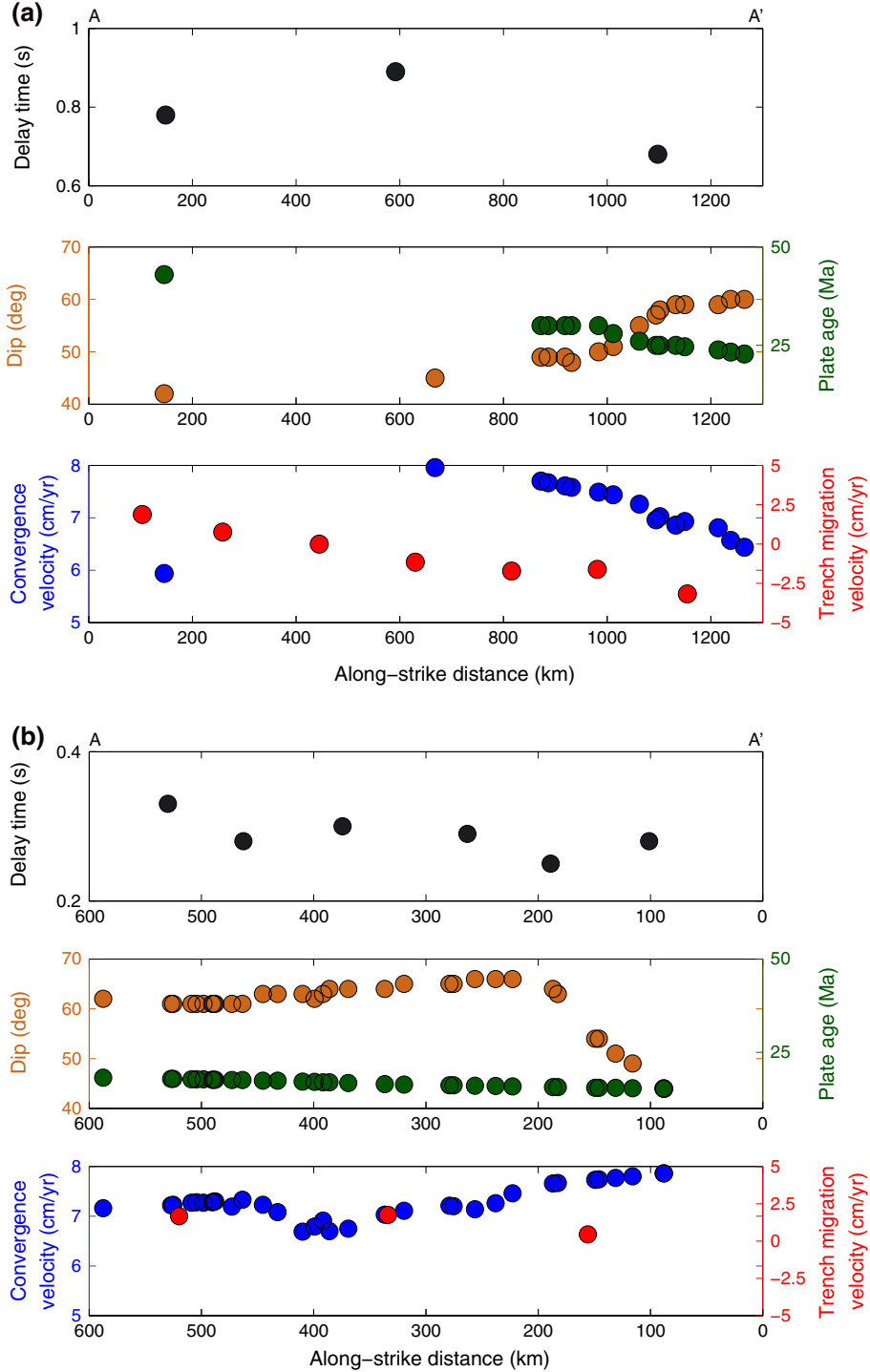


**Figure 8.** Variation of splitting delay times and other subduction parameters for the Ryukyu (a) and Central America (b) subduction zones. For each region, we show the along-strike variation in average  $\delta t$  (top panel), in plate age (green) and dip (orange) (middle panel), and in convergence velocity (blue) and trench migration velocity (red) (bottom panel). For trench migration velocity, positive values indicate trench rollback and negative values indicate trench advance.

LPO model and which show no obvious correlation. We also tested whether  $\delta t$  correlates with the along-strike component of ambient mantle flow to test the hypothesis that trench-parallel flow is driven by the global background mantle flow field; in this scenario, downgoing slabs are decoupled from the wedge above them and do not themselves represent the

major driver of wedge flow. We used values of large-scale flow derived from the global model of *Conrad and Behn* [2010] in a local fixed-trench reference frame, as compiled by *Paczkowski* [2012]. This comparison is shown in Figure 9c, and no obvious relationship is apparent. Finally, we investigated potential relationships between path-corrected

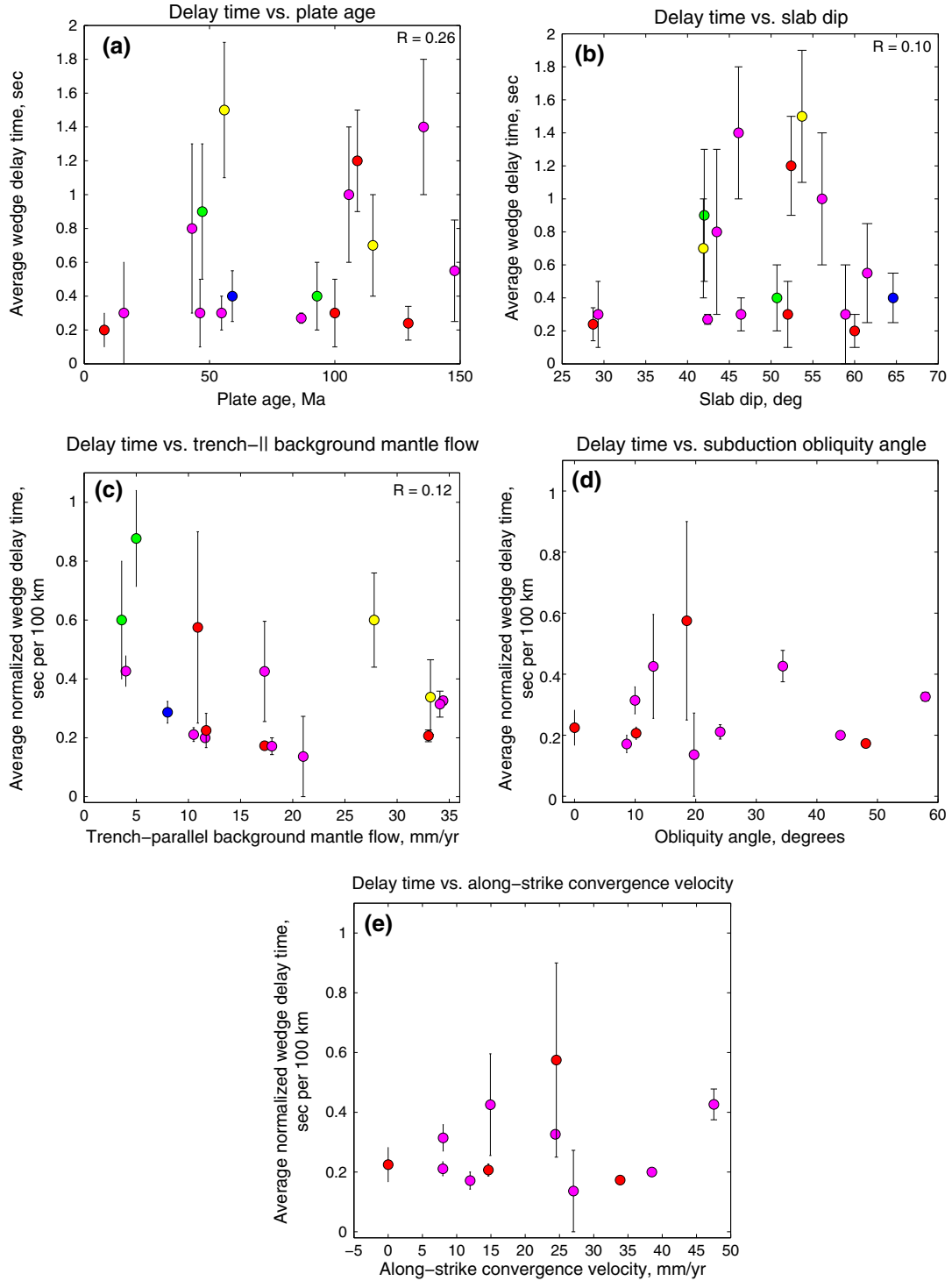


**Figure 9.** Additional plots of wedge delay times against various subduction parameters needed for specific testing of various models for wedge dynamics. In Figure 9a, we plot average wedge delay times (not corrected for path length) against downgoing plate age. In Figure 9b, we similarly plot non-corrected average delay times against slab dip. Figure 9c shows path-corrected average delay times versus the magnitude of the trench-parallel component of background mantle flow (including both the effects of trench migration and large-scale mantle convection, in the reference frame of the trench), as compiled by Paczkowski [2012]. In Figure 9d, we plot path-corrected average  $\delta t$  values against the obliquity angle of the subducting plate relative to the trench. Only systems with dominantly trench-parallel fast directions are shown (categories 1 and 2, as described in section 4.2). In Figure 9e, we similarly plot path-corrected delay times against the along-strike component of downgoing plate velocity (relative to the overriding plate); as in Figure 9d, we only show systems with dominantly trench-parallel  $\phi$ .

$\delta t$  and obliquity angle (Figure 9d) and path-corrected  $\delta t$  and along-strike downgoing plate velocity (Figure 9e) only for those systems with dominantly trench-parallel fast directions or systems that exhibit a trench-parallel to trench-perpendicular transition in  $\phi$ . This was intended to test the prediction of the oblique transpression model, and as with the other plots in Figure 9, we found no correlation between the sets of variables.

## 5. Discussion and Summary

[57] It is patently obvious from the tests and comparisons shown in Figures 7–9 that none of the predictions made by the simple models discussed in section 3 are supported by the global data set and that no model predicts the variations in wedge splitting behavior observed globally. To highlight just a few striking examples, the B-type fabric model predicts a transition from trench-parallel to trench-perpendicular fast directions approximately co-located with the volcanic arc, but while many systems do exhibit a transition at or near this location (Alaska, NE Japan, Mexico, and New Zealand), in the Tonga system the transition is located far into the back arc (~350 km from the trench), which is not consistent with the B-type fabric model. If trench-parallel flow driven by trench migration were the primary explanation for mantle wedge anisotropy, one might expect to see a relationship between  $\delta t$  (as a proxy for the strength/coherence of trench-parallel flow and the resulting anisotropy) and trench migration rate ( $V_t$  or  $|V_t|$ ). While there is a hint of a trend of increasing  $\delta t$  with increasing  $|V_t|$  for trenches moving faster than ~10 mm/yr (Figure 5o), a group of systems with nearly stationary trenches and large delay times (Figure 5o) does not agree with the predictions of this model.

[58] Some of the models discussed in section 3 are difficult to test directly with our global compilation but can be tested with regional datasets. For example, modeling studies have investigated the possibility of trench-parallel stretching in the mantle wedge due to complexity in slab morphology such as along-strike changes in slab dip [Kneller and van Keken, 2007, 2008]. We can gain some insight into whether this model of complex wedge flow due to complex slab morphology correctly describes the global wedge splitting data set by examining the plots in Figure 7 of along-strike variations in individual subduction zones. This figure includes Ryukyu, a relatively simple subduction system in terms of slab morphology. While the observations of complex splitting behavior in some systems are consistent with the predictions of the numerical models (e.g., South America and the Marianas) [Kneller et al., 2007], it is also clear that dominantly trench-parallel fast directions are also found in systems such as Ryukyu that exhibit relatively simple slab morphology. We can easily identify other wedge anisotropy mechanisms which very likely make a contribution in specific subduction zones but which do not appear to dominate the global signal. For example, antigorite LPO likely makes a major contribution in some subduction zones [Kneller et al., 2008; Nikulin et al., 2009] but certainly not all [e.g., Wirth and Long, 2012].

[59] There are some models that cannot be easily tested using typical local S splitting datasets but can be tested using the raypath configurations of specific studies. For example, aligned serpentinitized cracks in the shallow part of the slab

may be responsible for up to ~1 s of trench-parallel SKS splitting in some subduction zones [Faccenda et al., 2008]. The potential effect of such an SPO anisotropy on local S splitting measurements is somewhat ambiguous, as the effect on any given local S raypath would depend on the depth (relative to the interface at the top of the slab) of the source earthquake. One possibility is that for subduction systems with a well-defined double Wadati-Benioff zone (commonly known as a DBZ) [e.g., Brudzinski et al., 2007], rays that originate from the upper plane of seismicity would not sample the faulted, hydrated region of the slab, while rays that originate from the lower plane of seismicity would. Our global compilation of average splitting does not allow us to test this prediction, but a recent study by Huang et al. [2011b] used the well-defined DBZ beneath northeastern Japan to isolate the contribution to local S splitting from the shallow part of the slab and found that the contribution to splitting from the upper portion of the slab is limited to ~0.1 s. This prediction remains to be tested in other subduction zones, however.

[60] Rather than a single, simple model that explains the first-order characteristics of the global splitting data set, we favor a hybrid model that incorporates aspects of many of the models that have been proposed. Specifically, variables such as convergence velocity, trench migration, melt production, variations in slab morphology and wedge rheology, proximity to slab edges, ambient large-scale mantle flow, local mineralogy, and conditions of deformation all likely play a role in controlling wedge anisotropy. Such a hybrid conceptual model could and should be developed further into a model that makes specific testable predictions that are based on modeling of these various effects.

[61] If this complicated view of mantle wedge flow and anisotropy is correct, then there are some important implications for our understanding of wedge dynamics. To explore one example, along-strike material transport is likely important in many, though not all, mantle wedge systems. Such along-strike flow has important implications for our understanding of mantle wedge thermal structure, slab surface temperatures, and volatile and melt transport, phenomena which are usually investigated in the context of two-dimensional models. The effects of along-strike flow on phenomena such as slab surface temperatures or wedge thermal structure may serve as a testable prediction of a hybrid model. For instance, if the effects of along-strike flow on wedge thermal structure can be elucidated and predictions can be made about the effect on, say, geochemical or petrological observables, then independent lines of evidence for along-strike wedge flow can be tested against the patterns observed in the global wedge splitting data set. Another important implication of along-strike flow is the nature of mechanical coupling between slabs and the mantle material above them. In the sub-slab mantle, the possible presence of trench-parallel sub-slab flow has been inferred from anisotropy observations; if this view is correct, it implies some degree of mechanical decoupling between the slab and the subjacent mantle [Russo and Silver, 1994; Long and Silver, 2008, 2009; Jadamec and Billen, 2010; Paczkowski, 2012]. If such along-strike flow is present in the wedge as well, then it also implies that downgoing slabs are imperfectly coupled to the mantle above them, perhaps as a consequence of a strongly non-Newtonian rheology, the presence of partial melt, or the presence of weak materials such as serpentinites.

[62] In order to deepen our understanding of mantle wedge geodynamics and fully elucidate the many processes that may contribute to wedge anisotropy, it is vital to integrate the constraints from local  $S$  splitting studies such as those compiled in this paper with insights from geodynamics and mineral physics studies. To highlight one example, the viscosity structure of the mantle wedge remains one of the more poorly constrained parameters in subduction zone geodynamics [e.g., *van Keken*, 2003]. It is vital, however, to understanding the possible role of small-scale convection in wedge dynamics [*Wirth and Korenaga*, 2012] and to understanding how trench migration might drive along-strike material transport in the wedge [*Conder and Wiens*, 2007; *Druken et al.*, 2011]. Insights from geodynamical modeling [e.g., *Billen and Gurnis*, 2001; *Lev and Hager*, 2011] and mineral physics/petrology investigations [e.g., *Hirth and Kohlstedt*, 2003; *Dixon et al.*, 2004] are crucial to resolving the viscosity structure of the wedge and thus to understanding the controls on wedge flow. A second issue that cannot be resolved from shear wave splitting alone is the geometry of olivine and serpentinite LPO patterns under different conditions of deformation; understanding LPO geometry in different parts of the wedge system requires insight from both experiments [e.g., *Jung and Karato*, 2001; *Karato et al.*, 2008; *Katayama et al.*, 2009] and from natural mantle-derived rocks [e.g., *Mizukami et al.*, 2004; *Nishii et al.*, 2011]. Progress in our understanding of mantle wedge anisotropy and dynamics will not come from seismological investigations alone, of course, but requires integration of insights from multiple disciplines.

[63] Out of necessity, we have made many simplifying assumptions in assembling our compilation of first-order splitting patterns in subduction zone wedges worldwide, and no compilation of this type can capture all of the complexity inherent in any individual data set. However, our global compilation does have some advantages that circumvent some of the limitations of individual data sets (e.g., limited station and raypath coverage). For example, many individual local  $S$  splitting data sets lack the detail to discern a relationship between splitting delay time and event depth; however, such a relationship is visible in our global compilation (Figure 3). Although the tests and comparisons carried out here do not uniquely constrain all of the controls on mantle wedge anisotropy in subduction zones worldwide, we hope that our compilation will serve as a benchmark for future models of mantle wedge dynamics and for future work on, for example, the likely distribution of B-type olivine and deformed serpentinite above subducting slabs.

[64] The complexities in (and limitations of) local  $S$  splitting datasets and the many models for wedge anisotropy that are, to first order, consistent with observations have presented a major challenge for our understanding of wedge dynamics. While the comparisons between wedge splitting observations and subduction-related parameters presented in this paper can be helpful in ruling out certain models, it is clear that our understanding of the origin and implications of anisotropy in the mantle wedge is far from complete. We have argued in this paper that many factors—two-dimensional corner flow, along-strike flow, local complexities such as slab morphology, unusual LPO geometries in olivine and serpentinite minerals—likely compete to control the distribution of wedge anisotropy in any given subduction zone. While this complexity presents a major challenge, it

also presents an opportunity, because it implies that wedge anisotropy contains information about a host of subduction processes that are often difficult to constrain observationally. If our understanding of mantle wedge anisotropy progresses to the point where we can confidently assess the relative contributions of different processes in individual subduction systems, then observations and interpretations of anisotropic structure have the potential to yield important insights into mantle processes above subducting slabs.

[65] **Acknowledgments.** We sincerely thank the authors of the many studies used in our global compilation, without which this work would not be possible. We are grateful to Julia MacDougall for sharing results prior to publication. This work was supported by NSF via grant EAR-0911286 (MDL) and a Graduate Research Fellowship (EAW). Some figures were drafted using the Generic Mapping Tools [*Wessel and Smith*, 1991]. Several ideas explored in this paper were inspired by work done at the Department of Terrestrial Magnetism, Carnegie Institution of Washington, with the late Paul Silver. We thank Karen Fischer, an anonymous reviewer, and the Associate Editor for thorough and constructive reviews that greatly improved the manuscript.

## References

- Abers, G. A., P. E. van Keken, E. A. Kneller, A. Ferris, and J. C. Stachnik (2006), The thermal structure of subduction zones constrained by seismic imaging: Implications for slab dehydration and wedge flow. *Earth Planet. Sci. Lett.*, *241*, 387–397.
- Abt, D. L., and K. M. Fischer (2008), Resolving three-dimensional anisotropic structure with shear-wave splitting tomography. *Geophys. J. Int.*, *173*, 859–889.
- Abt, D. L., K. M. Fischer, G. A. Abers, W. Strauch, J. M. Protti, and V. Gonzalez (2009), Shear wave anisotropy beneath Nicaragua and Costa Rica: Implications for flow in the mantle wedge. *Geochem. Geophys. Geosyst.*, *10*, Q05S15, doi:10.1029/2009GC002375.
- Alsina, D., and R. Snieder (1995), Small-scale sublithospheric continental mantle deformation—Constraints from SKS splitting observations. *Geophys. J. Int.*, *123*, 431–448.
- Anderson, M. L., and G. Zandt (2004), Multiple layers of anisotropy in the Chile Argentina subduction zone. *Eos Trans. AGU*, *85*, Fall Meet. Suppl., Abstract T21B-0517.
- Anglin, K. D., and M. J. Fouch (2005), Seismic anisotropy in the Izu-Bonin subduction system. *Geophys. Res. Lett.*, *32*, L09307, doi:10.1029/2005GL022714.
- Audoine, E., M. K. Savage, and K. Gledhill (2004), Anisotropic structure under a back arc spreading region, the Taupo Volcanic Zone, New Zealand. *J. Geophys. Res.*, *109*, B11305, doi:10.1029/2003JB002932.
- Behn, M. D., G. Hirth, and P. B. Kelemen (2007), Trench-parallel anisotropy produced by foundering of arc lower crust. *Science*, *317*, 108–111.
- Bezacier, L., B. Reynard, J. D. Bass, C. Sanchez-Valle, and B. Van de Moortèle (2010), Elasticity of antigorite, seismic detection of serpentinites, and anisotropy in subduction zones. *Earth Planet. Sci. Lett.*, *289*, 198–208.
- Billen, M. I., and M. Gurnis (2001), A low viscosity wedge in subduction zones. *Earth Planet. Sci. Lett.*, *193*, 227–236.
- Bock, G., R. Kind, A. Rudloff, and G. Asch (1998), Shear wave anisotropy in the upper mantle beneath the Nazca plate in northern Chile. *J. Geophys. Res.*, *103*, 24,333–24,345.
- Bowman, J. R., and M. Ando (1987), Shear-wave splitting in the upper-mantle wedge above the Tonga subduction zone. *Geophys. J. Roy. Astr. Soc.*, *88*, 25–41.
- Brisbourne, A., G. Stuart, and J.-M. Kendall (1999), Anisotropic structure of the Hikurangi subduction zone, New Zealand—Integrated interpretation of surface-wave and body-wave observations. *Geophys. J. Int.*, *137*, 214–230.
- Brudzinski, M. R., C. H. Thurber, B. R. Hacker, and E. R. Engdahl (2007), Global prevalence of double Benioff zones. *Science*, *316*, 1472–1474.
- Buck, W. R. (1985), When does small-scale convection begin beneath oceanic lithosphere?. *Nature*, *313*, 775–777.
- Cagnioncle, A.-M., E. M. Parmentier, and L. T. Elkins-Tanton (2007), Effect of solid flow above a subducting slab on water distribution and melting at convergent plate boundaries. *J. Geophys. Res.*, *112*, B09402, doi:10.1029/2007JB004934.
- Christensen, D. H., G. A. Abers, and T. L. McKnight (2003), Mantle anisotropy beneath the Alaska range inferred from S-wave splitting observations: Results from BEAAR. *Eos Trans. AGU*, *84*, Fall Meet. Suppl., Abstract S31C-0782.

- Conder, J. A., and D. A. Wiens (2007), Rapid mantle flow beneath the Tonga volcanic arc, *Earth Planet. Sci. Lett.*, *264*, 299–307.
- Conrad, C. P., and M. D. Behn (2010), Constraints on lithosphere net rotation and asthenospheric viscosity from global mantle flow models and seismic anisotropy, *Geochem. Geophys. Geosyst.*, *11*, Q05W05, doi:10.1029/2009GC002970.
- Dewandel, B., F. Boudier, H. Kern, W. Warsi, and D. Mainprice (2003), Seismic wave velocity and anisotropy of serpentinized peridotite in the Oman ophiolite, *Tectonophysics*, *370*, 77–94.
- Dixon, J. E., T. H. Dixon, D. R. Bell, and R. Malservisi (2004), Lateral variation in upper mantle viscosity: Role of water, *Earth Planet. Sci. Lett.*, *222*, 451–467.
- Druken, K. A., M. D. Long, and C. Kincaid (2011), Mantle flow driven by slab rollback beneath the High Lava Plains, *Geophys. Res. Lett.*, *38*, L13310, doi:10.1029/2011GL047541.
- Eberhart-Phillips, D., and M. Reyners (2009), Three-dimensional distribution of seismic anisotropy in the Hikurangi subduction zone beneath the central North Island, New Zealand, *J. Geophys. Res.*, *114*, B06301, doi:10.1029/2008JB005947.
- Faccenda, M., and F. A. Capitanio (2012), Development of mantle seismic anisotropy during subduction-induced 3-D flow, *Geophys. Res. Lett.*, *39*, L11305, doi:10.1029/2012GL015988.
- Faccenda, M., L. Burlini, T. V. Gerya, and D. Mainprice (2008), Fault-induced seismic anisotropy by hydration in subducting oceanic plates, *Nature*, *455*, 1097–1100.
- Favier, N., and S. Chevrot (2003), Sensitivity kernels for shear wave splitting in transverse isotropic media, *Geophys. J. Int.*, *153*, 213–228.
- Fischer, K. M., and D. A. Wiens (1996), The depth distribution of mantle anisotropy beneath the Tonga subduction zone, *Earth Planet. Sci. Lett.*, *142*, 253–260.
- Fischer, K. M., M. J. Fouch, D. A. Wiens, and M. S. Boettcher (1998), Anisotropy and flow in Pacific subduction zone back-arcs, *Pure Appl. Geophys.* *151*, 463–475.
- Fouch, M. J., and K. M. Fischer (1996), Mantle anisotropy beneath northeast Pacific subduction zones, *J. Geophys. Res.*, *101*, 15,987–16,002.
- Fouch, M. J., and K. M. Fischer (1998), Shear wave anisotropy in the Mariana subduction zone, *Geophys. Res. Lett.*, *25*, 1221–1224.
- Gledhill, K., and D. Gubbins (1996), SKS splitting and the seismic anisotropy of the mantle beneath the Hikurangi subduction zone, New Zealand, *Phys. Earth Planet. Inter.* *95*, 227–236.
- Greve, S. M., M. K. Savage, and S. D. Hofmann (2008), Strong variations in seismic anisotropy across the Hikurangi subduction zone, North Island, New Zealand, *Tectonophysics*, *462*, 7–21.
- Grove, T. L., C. B. Till, E. Lev, N. Chatterjee, and E. Médard (2009), Kinematic variables and water transport control the formation and location of arc volcanoes, *Nature*, *459*, 694–697.
- Hall, C., K. M. Fischer, E. M. Parmentier, and D. K. Blackman (2000), The influence of plate motions on three-dimensional back arc mantle flow and shear wave splitting, *J. Geophys. Res.*, *105*, 28,009–28,033.
- Hammond, J. O. S., J. Wookey, S. Kaneshima, H. Inoue, T. Yamashina, and P. Harjadi (2010), Systematic variation in anisotropy beneath the mantle wedge in the Java-Sumatra subduction system from shear wave splitting, *Phys. Earth Planet. Inter.*, *178*, 189–201.
- Healy, D., S. M. Reddy, N. E. Timms, E. M. Gray, and A. V. Brovarone (2009), Trench-parallel fast axes of seismic anisotropy due to fluid-filled cracks in subducting slabs, *Earth Planet. Sci. Lett.*, *238*, 75–86.
- Heuret, A., and S. Lallemand (2005), Plate motions, slab dynamics and back-arc deformation, *Phys. Earth Planet. Inter.*, *149*, 31–51.
- Heyworth, Z., K. M. Knesel, S. P. Turner, and R. J. Arculus (2011), Pb-isotopic evidence for rapid trench-parallel mantle flow beneath Vanuatu, *J. Geol. Soc.*, *168*, 265–271.
- Hilalret, N., and B. Reynard (2008), Stability and dynamics of serpentine layer in subduction zone, *Tectonophysics*, *465*, 24–29.
- Hirth, G., and D. Kohlstedt (2003), Rheology of the upper mantle and the mantle wedge: A view from the experimentalists, in *Inside the subduction factory*, edited by J. Eiler, pp. 83–105, American Geophysical Union, Washington, DC.
- Hoernle, K., D. L. Abt, K. M. Fischer, H. Nichols, F. Hauff, G. A. Abers, P. van der Bogard, K. Heydolph, G. Alvarado, M. Protti, and W. Strauch (2008), Geochemical and geophysical evidence for arc-parallel flow in the mantle wedge beneath Costa Rica and Nicaragua, *Nature*, *451*, 1094–1098.
- Holtzman, B. K., and J.-M. Kendall (2010), Organized melt, seismic anisotropy, and plate boundary lubrication, *Geochem. Geophys. Geosyst.*, *11*, Q0AB06, doi:10.1029/2010GC003296.
- Holtzman, B. K., D. L. Kohlstedt, M. E. Zimmerman, F. Heidelbach, T. Hiraga, and J. Hustoft (2003), Melt segregation and strain partitioning: Implications for seismic anisotropy and mantle flow, *Science*, *301*, 1227–1230.
- Honda, S. (2011), Planform of small-scale convection under the island arc, *Geochem. Geophys. Geosyst.*, *12*, Q11005, doi:10.1029/2011GC003827.
- Honda, S., and T. Yoshida (2005), Application of the model of small-scale convection under the island arc to the NE Honshu subduction zone, *Geochem. Geophys. Geosyst.*, *6*, Q01002, doi:10.1029/2004GC000785.
- Huang, Z., D. Zhao, and L. Wang (2011a), Frequency-dependent shear-wave splitting and multilayer anisotropy in northeast Japan, *Geophys. Res. Lett.*, *38*, L08302, doi:10.1029/2011GL046804.
- Huang, Z., D. Zhao, and L. Wang (2011b), Shear wave anisotropy in the crust, mantle wedge, and subducting Pacific slab under northeast Japan, *Geochem. Geophys. Geosyst.*, *12*, Q01002, doi:10.1029/2010GC003343.
- Jadamec, M. A., and M. I. Billen (2010), Reconciling surface plate motions with rapid three-dimensional mantle flow around a slab edge, *Nature*, *465*, 338–341.
- Jarrard, R. D. (1986), Relations among subduction parameters, *Rev. Geophys.*, *24*, 217–284.
- Jung, H. (2011), Seismic anisotropy produced by serpentine in mantle wedge, *Earth Planet. Sci. Lett.*, *307*, 535–543.
- Jung, H., and S.-i. Karato (2001), Water-induced fabric transitions in olivine, *Science*, *293*, 1460–1463.
- Jung, H., I. Katayama, Z. Jiang, T. Hiraga, and S. Karato (2006), Effect of water and stress on the lattice-preferred orientation of olivine, *Tectonophysics*, *421*, 1–22.
- Kaminski, E., and N. M. Ribe (2002), Timescales for the evolution of seismic anisotropy in mantle flow, *Geochem. Geophys. Geosyst.*, *3*, 1051, doi:10.1029/2001GC000222.
- Kaneshima, S. and P. G. Silver (1995), Anisotropic loci in the mantle beneath central Peru, *Phys. Earth Planet. Inter.*, *88*, 257–272.
- Karato, S.-i., H. Jung, I. Katayama, and P. Skemer (2008), Geodynamic significance of seismic anisotropy of the upper mantle: New insights from laboratory studies, *Annu. Rev. Earth Planet. Sci.*, *36*, 59–95.
- Katayama, I. (2009), Thin anisotropic layer in the mantle wedge beneath northeast Japan, *Geology*, *37*, 211–214.
- Katayama, I., K.-i. Hirauchi, K. Michibayashi, and J.-i. Ando (2009), Trench-parallel anisotropy produced by serpentine deformation in the hydrated mantle wedge, *Nature*, *461*, 1114–1117.
- Kelemen, P. B., J. L. Rilling, E. M. Parmentier, L. Mehl, and B. R. Hacker (2003), Thermal structure due to solid-state flow in the mantle wedge beneath arcs, in *Inside the Subduction Factory*, edited by J. Eiler, pp. 293–311, American Geophysical Union, Washington, DC.
- Kern H. (1993), P- and S-wave anisotropy and shear-wave splitting at pressure and temperature in possible mantle rocks and their relation to the rock fabric, *Phys. Earth Planet. Inter.*, *78*, 245–256.
- Kincaid, C., and I. S. Sacks (1997), Thermal and dynamical evolution of the upper mantle in subduction zones, *J. Geophys. Res.*, *102* (B6), 12,295–12,315, doi:10.1029/96JB03553.
- Kneller, E. A., and P. E. van Keken (2007), Trench-parallel flow and seismic anisotropy in the Marianas and Andean subduction systems, *Nature*, *450*, 1222–1225.
- Kneller, E. A., and P. E. van Keken (2008), The effects of three-dimensional slab geometry on deformation in the mantle wedge: Implications for shear wave anisotropy, *Geochem. Geophys. Geosyst.*, *9*, doi:10.1029/2007GC001677.
- Kneller, E. A., P. E. van Keken, S. Karato, and J. Park (2005), B-type olivine fabric in the mantle wedge: Insights from high-resolution non-Newtonian subduction zone models, *Earth Planet. Sci. Lett.*, *237*, 781–797.
- Kneller, E. A., P. E. van Keken, I. Katayama, and S. Karato (2007), Stress, strain, and B-type olivine fabric in the fore-arc mantle: Sensitivity tests using high-resolution steady-state subduction zone models, *J. Geophys. Res.*, *112*, B04406, doi:10.1029/2006JB004544.
- Kneller, E. A., M. D. Long, and P. E. van Keken (2008), Olivine fabric transitions and shear-wave anisotropy in the Ryukyu subduction system, *Earth Planet. Sci. Lett.*, *268*, 268–282.
- Korenaga, J., and T. H. Jordan (2003), Physics of multiscale convection in Earth's mantle: Onset of sublithospheric convection, *J. Geophys. Res.*, *108*, 2333, doi:10.1029/2002JB001760.
- Lallemand, S., A. Heruret, C. Faccenna, and F. Funiciello (2008), Subduction dynamics as revealed by trench migration, *Tectonics*, *27*, doi:10.1029/2007TC002212.
- Landuyt, W., and G. Ierley (2012), Linear stability analysis of the onset of sublithospheric convection, *Geophys. J. Int.*, *189*, 19–28.
- Lassak, T. M., M. J. Fouch, C. E. Hall, and E. Kaminski (2006), Seismic characterization of mantle flow in subduction systems: Can we resolve a hydrated mantle wedge? *Earth Planet. Sci. Lett.*, *243*, 632–649.
- Léon Soto, G., J. F. Ni, S. P. Grand, E. Sandvol, R. W. Valenzuela, M. Guzmán Speziale, J. M. Gómez González, and T. Domínguez Reyes (2009), Mantle flow in the Rivera-Cocos subduction zone. *Geophys. J. Int.*, *179*, 1004–1012.
- Lev, E., and B. H. Hager (2011), Anisotropic viscosity changes subduction zone thermal structure, *Geochem. Geophys. Geosyst.*, *12*, Q04009, doi:10.1029/2010GC003382.

- Levin, V., and J. Park (1998), P-SH conversions in layered media with hexagonally symmetric anisotropy: A cookbook, *Pure Appl Geophys.*, *151*, 669–697.
- Levin, V., D. Droznin, J. Park, and E. Gordeev (2004), Detailed mapping of seismic anisotropy with local shear waves in southeastern Kamchatka, *Geophys. J. Int.*, *158*, 1009–1023.
- Levin, V., D. Okaya, and J. Park (2007), Shear wave birefringence in wedge-shaped anisotropic regions, *Geophys. J. Int.*, *168*, 275–286.
- Long, M. D., B. H. Hager, M. V. de Hoop, and R. D. van der Hilst (2007), Two-dimensional modeling of subduction zone anisotropy and application to southwestern Japan, *Geophys. J. Int.*, *170*, 839–856.
- Long, M. D., and P. G. Silver (2008), The subduction zone flow field from seismic anisotropy: A global view, *Science*, *319*, 315–318.
- Long, M. D., and P. G. Silver (2009), Mantle flow in subduction systems: The sub-slab flow field and implications for mantle dynamics, *J. Geophys. Res.*, *114*, B10312, doi:10.1029/2008JB006200.
- Long, M. D., and R. D. van der Hilst (2006), Shear wave splitting from local events beneath the Ryukyu arc: Trench-parallel anisotropy in the mantle wedge, *Phys. Earth Planet. Inter.*, *155*, 300–312.
- Long, M. D., and T. W. Becker (2010), Mantle dynamics and seismic anisotropy, *Earth Planet. Sci. Lett.*, *297*, 341–354.
- MacDougall, J. G., K. M. Fischer, and M. L. Anderson (2012), Seismic anisotropy above and below the subducting Nazca lithosphere in southern South America, *J. Geophys. Res.*, *117*, B12306, doi:10.1029/2012JB009538.
- Mainprice, D., and B. Ildefonse (2009), Seismic anisotropy of subduction zone minerals—Contribution of hydrous phases, in *Subduction Zone Geodynamics*, edited by S. Lallemand, and F. Funicello, pp. 63–84, Springer-Verlag, Berlin Heidelberg.
- Marson-Pidgeon, K., and M. K. Savage (1997), Frequency-dependent anisotropy in Wellington, New Zealand, *Geophys. Res. Lett.*, *24*, 3297–3300.
- Marson-Pidgeon K., and M. K. Savage (2004), Shear-wave splitting variations across an array in the southern North Island, New Zealand, *Geophys. Res. Lett.*, *31*, L21602, doi:10.1029/2004GL021190.
- Matcham, I., M. K. Savage, and K. R. Gledhill (2000), Distribution of seismic anisotropy in the subduction zone beneath the Wellington, New Zealand, *Geophys. J. Int.*, *140*, 1–10.
- McKenzie, D. (1979), Finite deformation during fluid flow, *Geophys. J. Roy. Astron. Soc.*, *58*, 689–715.
- Mehl, L., B. R. Hacker, G. Hirth, and P. B. Kelemen (2003), Arc-parallel flow within the mantle wedge: Evidence from the accreted Talkeetna arc, south central Alaska, *J. Geophys. Res.*, *108*, 2375, doi:10.1029/2002JB002233.
- Mizukami, T., S. R. Wallis, and J. Yamamoto (2004), Natural examples of olivine lattice preferred orientation patterns with a flow-normal a-axis maximum, *Nature*, *427*, 432–436.
- Mookherjee, M., and G. C. Capitani (2011), Trench parallel anisotropy and large delay times: Elasticity and anisotropy of antigorite at high pressures, *Geophys. Res. Lett.*, *38*, L09315, doi:10.1029/2011GL047160.
- Morishege, M., and S. Honda (2011), Three-dimensional structure of P-wave anisotropy in the presence of small-scale convection in the mantle wedge, *Geochem. Geophys. Geosyst.*, *12*, Q12010, doi:10.1029/2011GC003866.
- Morley, A. M., G. W. Stuart, J.-M. Kendall, and M. Reyners (2006), Mantle wedge anisotropy in the Hikurangi subduction zone, central North Island, New Zealand, *Geophys. Res. Lett.*, *33*, L05301, doi:10.1029/2005GL024569.
- Müller, C. (2001), Upper mantle seismic anisotropy beneath Antarctica and the Scotia Sea region, *Geophys. J. Int.*, *147*, 105–122.
- Nakajima, J., and A. Hasegawa (2004), Shear-wave polarization anisotropy and subduction-induced flow in the mantle wedge of northern Japan, *Earth Planet. Sci. Lett.*, *225*, 365–377.
- Nakajima, J., J. Shimizu, S. Hori, and A. Hasegawa (2006), Shear-wave splitting beneath the southwestern Kurile arc and northeastern Japan arc: A new insight into mantle return flow, *Geophys. Res. Lett.*, *33*, L05305, doi:10.1029/2005GL025053.
- Nikulin, A., V. Levin, and J. Park (2009), Receiver function study of the Cascadia megathrust: Evidence for localized serpentinization, *Geochem. Geophys. Geosyst.*, *10*, Q07004, doi:10.1029/2009GC002376.
- Nishii, A., S. R. Wallis, T. Mizukami, and K. Michibayashi (2011), Subduction related antigorite CPO patterns from forearc mantle in the Sanbagawa belt, southwest Japan, *J. Struct. Geol.*, *33*, 1436–1445.
- Okada, T., T. Matsuzawa, and A. Hasegawa (1995), Shear-wave polarization anisotropy beneath the north-eastern part of Honshu, Japan, *Geophys. J. Int.*, *123*, 781–797.
- Paczkowski, K. (2012), Dynamic analysis of modifications to simple plate tectonic theory. Ph.D. Thesis, Yale University, 185 pp.
- Park, J., H. Yuan, and V. Levin (2004), Subduction-zone anisotropy under Corvallis, Oregon: A serpentine skidmark of trench-parallel terrane migration? *J. Geophys. Res.*, *109*, B10306, doi:10.1029/2003JB002718.
- Piñero-Felicangeli, L., and J.-M. Kendall (2008), Sub-slab mantle flow parallel to the Caribbean plate boundaries: Inferences from SKS splitting, *Tectonophysics*, *462*, 22–34.
- Polet, J., P. G. Silver, S. Beck, T. Wallace, G. Zandt, S. Ruppert, R. Kind, and A. Rudloff (2000), Shear wave anisotropy beneath the Andes from the BANJO, SEDA, and PISCO experiments, *J. Geophys. Res.*, *105*, 6287–6304.
- Pozgay, S. H., D. A. Wiens, J. A. Conder, H. Shiobara, and H. Sugioka (2007), Complex mantle flow in the Mariana subduction system: Evidence from shear wave splitting, *Geophys. J. Int.*, *170*, 371–386.
- Ranero, C. R., J. Phipps Morgan, K. McIntish, and C. Reichert (2003), Bending-related faulting and mantle serpentinization at the Middle America trench, *Nature*, *425*, 367–373.
- Reymer, A., and G. Schubert (1984), Phanerozoic addition rates to the continental crust and crustal growth, *Tectonics*, *3*, 63–77.
- Richter, F. M., and B. Parsons (1975), On the interaction of two scales of convection in the mantle, *J. Geophys. Res.*, *80*, 2529–2541.
- Russo, R. M., and P. G. Silver (1994), Trench-parallel flow beneath the Nazca plate from seismic anisotropy, *Science*, *263*, 1105–1111.
- Salah, M. K., T. Seno, and T. Iidaka (2008), Upper mantle anisotropy beneath central and southwest Japan: An insight into subduction-induced mantle flow, *J. Geodyn.*, *46*, 21–37.
- Salah, M. K., T. Seno, and T. Iidaka (2009), Seismic anisotropy in the wedge above the Philippine Sea slab beneath Kanto and southwest Japan derived from shear wave splitting, *J. Asian Earth Sci.*, *34*, 61–75.
- Savage, M. K. (1999), Seismic anisotropy and mantle deformation: What have we learned from shear wave splitting?, *Rev. Geophys.*, *37*, 65–106.
- Schellart, W. P., D. R. Stegman, and J. Freeman (2008), Global trench migration velocities and slab migration induced upper mantle volume fluxes: Constraints to find an Earth reference frame based on minimizing viscous dissipation, *Earth-Science Rev.*, *88*, 118–144.
- Smith, G. P., D. A. Wiens, K. M. Fischer, L. M. Dorman, S. C. Webb, and J. A. Hildebrand (2001), A complex pattern of mantle flow in the Lau Backarc, *Science*, *292*, 713–716.
- Syracuse, E., and G. Abers (2006), Global compilation of variations in slab depth beneath arc volcanoes and implications, *Geochem. Geophys. Geosyst.*, *7*, doi:10.1029/2005GC001045.
- Tasaka, M., K. Michibayashi, and D. Mainprice (2008), B-type olivine fabrics developed in the fore-arc side of the mantle wedge along a subducting slab, *Earth Planet. Sci. Lett.*, *272*, 747–757.
- Tian, Y., and D. Zhao (2012), Seismic anisotropy and heterogeneity in the Alaska subduction zone, *Geophys. J. Int.*, doi:10.1111/j.1365-246X.2012.05512.x.
- Tono, Y., Y. Fukao, T. Kunugi, and S. Tsuboi (2009), Seismic anisotropy of the Pacific slab and mantle wedge beneath the Japanese islands, *J. Geophys. Res.*, *114*, B07307, doi:10.1029/2009JB006290.
- Tovish, A., and G. Schubert (1978), Island arc curvature, velocity of convergence and angle of subduction, *Geophys. Res. Lett.*, *5*, 329–332.
- Turcotte, D. L. and G. Schubert (1982), *Geodynamics: Applications of Continuum Physics to Geological Problems*, John Wiley & Sons, New York, NY.
- Turner, S., and C. Hawkesworth (1998), Using geochemistry to map mantle flow beneath the Lau Basin, *Geology*, *26*, 1019–1022.
- van de Moortèle, B., L. Bezacier, G. Trullenque, and B. Reynard (2010), Electron back-scattering diffraction (EBSD) measurements of antigorite lattice-preferred orientation (LPO), *J. Microscopy*, *239*, 245–248.
- van Keken, P. E. (2003), The structure and dynamics of the mantle wedge, *Earth Planet. Sci. Lett.*, *215*, 323–338.
- van Keken, P. E., B. Keifer, and S. M. Peacock (2002), High-resolution models of subduction zones: Implications for mineral dehydration reactions and the transport of water into the deep mantle, *Geochem. Geophys. Geosyst.*, *3*(10), 1056, doi:10.1029/2001GC000256.
- Vauchez, A., A. Tommasi, G. Barruol, and J. Maumus (2000), Upper mantle deformation and seismic anisotropy in continental rifts, *Phys. Chem. Earth A*, *25*, 111–117.
- Volti, T., A. Gorbato, H. Shiobara, H. Sugioka, K. Mochizuki, and Y. Kaneda (2006), Shear-wave splitting in the Mariana trough—A relation between back-arc spreading and mantle flow? *Earth Planet. Sci. Lett.*, *244*, 566–575.
- Wang, J., and D. Zhao (2008), P wave anisotropic tomography beneath Northeast Japan, *Phys. Earth Planet. Inter.*, *170*, 115–133.
- Wang, J., and D. Zhao (2012), P wave anisotropic tomography of the Nankai subduction zone in Southwest Japan, *Geochem. Geophys. Geosyst.*, *13*, Q05017, doi:10.1029/2012GC004081.
- Wessel, P., and W. H. F. Smith (1991), Free software helps map and display data, *Eos Trans. AGU*, *72*, 441, doi:10.1029/90EO00319.
- Wiens, D. A., and G. P. Smith (2003), Seismological constraints on structure and flow patterns within the mantle wedge, in *Inside the Subduction Factory*, edited by J. Eiler, pp. 59–81, American Geophysical Union, Washington, DC.

## LONG AND WIRTH: MANTLE WEDGE ANISOTROPY

- Wiens, D. A., J. A. Conder, and U. H. Faul (2008), The seismic structure and dynamics of the mantle wedge, *Annu. Rev. Earth Planet. Sci.*, *36*, 421–455.
- Wirth, E. A., and J. Korenaga (2012), Small-scale convection in the subduction zone mantle wedge, *Earth Planet. Sci. Lett.*, *357–358*, 111–118.
- Wirth, E., and M. D. Long (2010), Frequency dependent shear wave splitting beneath the Japan and Izu-Bonin subduction zones. *Phys. Earth Planet. Inter.*, *181*, 141–154.
- Wirth, E. A., and M. D. Long (2012), Multiple layers of seismic anisotropy and a low-velocity layer in the mantle wedge beneath Japan: Evidence from teleseismic receiver functions, *Geochem. Geophys. Geosyst.*, *13*, Q08005, doi:10.1029/2012GC004180.
- Zhang, S., and S. Karato (1995), Lattice preferred orientation of olivine aggregates deformed in simple shear, *Nature*, *415*, 777–780.
- Zimmerman, M. E., S. Zhang, D. L. Kohlstedt, and S. Karato (1999), Melt distribution in mantle rocks deformed in simple shear, *Geophys. Res. Lett.*, *26*, 1505–1508.